Title
Construction of periodic adapted orthonormal frames on closed space curves

Permalink
https://escholarship.org/uc/item/49b224r8

Authors
Farouki, Rida T
Kim, Soo Hyun
Moon, Hwan Pyo

Peer reviewed

Construction of periodic adapted orthonormal frames on closed space curves

Rida T. Farouki

Department of Mechanical and Aerospace Engineering,
University of California, Davis, CA 95616, USA

Soo Hyun Kim and Hwan Pyo Moon
Department of Mathematics,
Dongguk University–Seoul, Seoul 04620, Republic of Korea

Abstract

The construction of continuous adapted orthonormal frames along C^1 closed–loop spatial curves is addressed. Such frames are important in the design of periodic spatial rigid–body motions along smooth closed paths. The construction is illustrated through the simplest non–trivial context — namely, C^1 closed loops defined by a single Pythagorean–hodograph (PH) quintic space curve of a prescribed total arc length. It is shown that such curves comprise a two–parameter family, dependent on two angular variables, and they degenerate to planar curves when these parameters differ by an integer multiple of π. The desired frame is constructed through a rotation applied to the normal–plane vectors of the *Euler–Rodrigues frame*, so as to interpolate a given initial/final frame orientation. A general solution for periodic adapted frames of minimal twist on C^1 closed–loop PH curves is possible, although this incurs transcendental terms. However, the C^1 closed–loop PH quintics admit particularly simple rational periodic adapted frames.

e–mail: farouki@ucdavis.edu, sookim@dongguk.edu, hpmoon@dongguk.edu

1   Introduction

The specification of orientational constraints along smooth space curves is a basic problem in spatial kinematics. For a curve $\mathbf{r}(\xi)$ defined by a polynomial or rational parameterization, orientation may be specified by an orthonormal frame $(\mathbf{f}_1(\xi), \mathbf{f}_2(\xi), \mathbf{f}_3(\xi))$, and a rational dependence of the frame on the curve parameter ξ is desirable. An *adapted frame* employs the curve tangent $\mathbf{t}(\xi) = \mathbf{r}'(\xi)/|\mathbf{r}'(\xi|$ as the vector $\mathbf{f}_1(\xi)$, while $\mathbf{f}_2(\xi), \mathbf{f}_3(\xi)$ span the normal plane. For a *rational* adapted frame, $\mathbf{r}(\xi)$ should be a *Pythagorean–hodograph* (PH) *curve*, since only PH curves possess rational unit tangents [5].

Along a spatial path $\mathbf{r}(\xi)$, the variation of an adapted frame is described by its angular velocity $\boldsymbol{\omega}$ through the differential relations

$$\frac{\mathrm{d}\mathbf{f}_1}{\mathrm{d}s} = \boldsymbol{\omega} \times \mathbf{f}_1 \,, \quad \frac{\mathrm{d}\mathbf{f}_2}{\mathrm{d}s} = \boldsymbol{\omega} \times \mathbf{f}_2 \,, \quad \frac{\mathrm{d}\mathbf{f}_3}{\mathrm{d}s} = \boldsymbol{\omega} \times \mathbf{f}_3 \,,$$

where s denotes arc length along $\mathbf{r}(\xi)$. The angular velocity may be expressed in terms of components relative to the frame itself as $\boldsymbol{\omega} = \omega_1\mathbf{f}_1 + \omega_2\mathbf{f}_2 + \omega_3\mathbf{f}_3$, and the constraint expressed by $\omega_1 \equiv 0$ identifies a *rotation–minimizing frame* (RMF), wherein the normal–plane vectors $\mathbf{f}_2$ and $\mathbf{f}_3$ exhibit no instantaneous rotation about the tangent $\mathbf{f}_1$. The rotation–minimizing frames — also called *Bishop frames* [2] — are of great importance in swept surface constructions, robot path planning, 5–axis CNC machining, and related applications. Many schemes for the approximation of RMFs on space curves have been proposed, and recently the focus has been [1, 3, 6, 10, 11, 14, 16, 17] on identifying curves that admit *rational* RMFs — see [7] for a survey of these developments.

The construction of an RMF on a space curve corresponds to solving an *initial value problem* [19] — i.e., specifying the frame orientation at any point of the curve determines its orientation at every other point. Consequently, an RMF cannot match freely–specified initial *and* final orientations for a rigid–body motion along a prescribed space curve. To address this limitation of the RMF, the concept of a *minimal–twist frame* (MTF) has been introduced [15]. An MTF matches specified initial and final frame orientations on a pre–determined curve, with a consistent sense of the angular velocity component ω_1 between them, and the least value of its integral with respect to arc length. Methods for constructing *rational* MTFs on spatial PH curves of degree 5 and 7 have been proposed in [12] and [15]. Moreover, these methods minimize the squared deviation of ω_1 about its mean value.

Prior studies of adapted frames on PH space curves have focused on open paths $\mathbf{r}(\xi)$, $\xi \in [\,0,1\,]$ with $\mathbf{r}(1) \neq \mathbf{r}(0)$. We consider here closed C^1 paths with

$\mathbf{r}(1) = \mathbf{r}(0)$ and $\mathbf{r}'(1) = \mathbf{r}'(0)$, and we wish to guarantee matched initial/final frames, $(\mathbf{f}_1(1), \mathbf{f}_2(1), \mathbf{f}_3(1)) = (\mathbf{f}_1(0), \mathbf{f}_2(0), \mathbf{f}_3(0))$, at the juncture point. This adapted frame periodicity is *not* (in general) satisfied by the RMF.

The plan for the remainder of this paper is as follows. First, Section 2 briefly reviews some salient features of the quaternion and Hopf map forms of spatial PH curves. Section 3 then introduces a novel two–parameter family of non–planar C^1 closed curves consisting of a single PH quintic segment, and elucidates their properties. Section 4 introduces the *phase angle* function between two adapted frames on a given space curve and the *angle discrepancy* of a single adapted frame on a C^1 closed curve, and employs them to construct periodic MTFs along the C^1 PH quintic closed loops identified in Section 3. Section 5 then describes a simple method for constructing *rational* adapted frames with C^1 periodicity on C^1 PH quintic closed loops. Finally, Section 6 recapitulates the main results of this study, and identifies further desirable developments of the methodology proposed herein.

2   Spatial Pythagorean-hodograph curves

The *quaternion* and *Hopf map* forms [4, 9] are alternative (equivalent) models for the construction of spatial PH curves. The former generates a Pythagorean hodograph $\mathbf{r}'(\xi)$ from a quaternion[1] polynomial

$$\mathcal{A}(\xi) \,=\, u(\xi) + v(\xi)\,\mathbf{i} + p(\xi)\,\mathbf{j} + q(\xi)\,\mathbf{k} \tag{1}$$

and its conjugate $\mathcal{A}^*(\xi) = u(\xi) - v(\xi)\,\mathbf{i} - p(\xi)\,\mathbf{j} - q(\xi)\,\mathbf{k}$ through the product[2]

$$\begin{aligned}
\mathbf{r}'(\xi) \,=\, \mathcal{A}(\xi)\,\mathbf{i}\,\mathcal{A}^*(\xi) \,=\, & [\,u^2(\xi) + v^2(\xi) - p^2(\xi) - q^2(\xi)\,]\,\mathbf{i} \\
& + 2\,[\,u(\xi)q(\xi) + v(\xi)p(\xi)\,]\,\mathbf{j} \,+\, 2\,[\,v(\xi)q(\xi) - u(\xi)p(\xi)\,]\,\mathbf{k}\,,
\end{aligned} \tag{2}$$

and the latter generates a Pythagorean hodograph from complex polynomials

$$\boldsymbol{\alpha}(\xi) \,=\, u(\xi) + \mathrm{i}\,v(\xi)\,, \quad \boldsymbol{\beta}(\xi) \,=\, q(\xi) + \mathrm{i}\,p(\xi) \tag{3}$$

through the expression

$$\mathbf{r}'(\xi) \,=\, (\,|\boldsymbol{\alpha}(\xi)|^2 - |\boldsymbol{\beta}(\xi)|^2,\, 2\,\mathrm{Re}(\boldsymbol{\alpha}(\xi)\overline{\boldsymbol{\beta}}(\xi)),\, 2\,\mathrm{Im}(\boldsymbol{\alpha}(\xi)\overline{\boldsymbol{\beta}}(\xi)))\,. \tag{4}$$

---

[1]Calligraphic characters such as $\mathcal{A}$ are used to denote quaternions, their scalar (real) and vector (imaginary) parts being denoted by $\mathrm{scal}(\mathcal{A})$ and $\mathrm{vect}(\mathcal{A})$. Bold symbols denote either complex numbers or vectors in $\mathbb{R}^3$ — the meaning should be clear from the context.

[2]Note that products of the form $\mathcal{A}\,\mathbf{i}\,\mathcal{A}^*$ always generate pure vector quaternions.

The parametric speed (i.e., the derivative $\mathrm{d}s/\mathrm{d}\xi$ of arc length s with respect to the curve parameter ξ) is defined in these two representations by

$$\sigma(\xi) \;=\; |\mathbf{r}'(\xi)| \;=\; |\mathcal{A}(\xi)|^2 \;=\; |\boldsymbol{\alpha}(\xi)|^2 + |\boldsymbol{\beta}(\xi)|^2\,.$$

The equivalence of (2) and (4) can be seen by setting $\mathcal{A}(\xi) = \boldsymbol{\alpha}(\xi) + \mathbf{k}\,\boldsymbol{\beta}(\xi)$, where the imaginary unit i is identified with the quaternion basis element $\mathbf{i}$. It is advantageous to simultaneously employ both the forms (2) and (4) — the Hopf map form yields a simpler expression for the imposition of arc length constraints, but the quaternion form is somewhat more convenient in formulating algorithms to construct PH curve interpolants.

The *Euler–Rodrigues frame* (ERF) is an adapted orthonormal frame that is defined on any spatial PH curve [4] through the rational expressions

$$(\mathbf{e}_1(\xi), \mathbf{e}_2(\xi), \mathbf{e}_3(\xi)) \;=\; \frac{(\mathcal{A}(\xi)\,\mathbf{i}\,\mathcal{A}^*(\xi), \mathcal{A}(\xi)\,\mathbf{j}\,\mathcal{A}^*(\xi), \mathcal{A}(\xi)\,\mathbf{k}\,\mathcal{A}^*(\xi))}{|\mathcal{A}(\xi)|^2}\,, \qquad (5)$$

wherein $\mathbf{e}_1(\xi)$ is the curve tangent, while $\mathbf{e}_2(\xi), \mathbf{e}_3(\xi)$ span the normal plane. The ERF angular velocity may be expressed as $\boldsymbol{\omega} = \omega_1 \mathbf{e}_1 + \omega_2 \mathbf{e}_2 + \omega_3 \mathbf{e}_3$, and we are primarily interested in the tangent component ω_1, which specifies the rate of rotation of $\mathbf{e}_2(\xi)$ and $\mathbf{e}_3(\xi)$ about $\mathbf{e}_1(\xi)$. This component may be expressed [7] as

$$\omega_1(\xi) \;=\; 2\,\frac{h(\xi)}{\sigma^2(\xi)}\,, \qquad (6)$$

where $h(\xi)$ is the polynomial specified in terms of the components of (1) or (3) as

$$h(\xi) \;=\; u(\xi)v'(\xi) - u'(\xi)v(\xi) - p(\xi)q'(\xi) + p'(\xi)q(\xi)\,. \qquad (7)$$

3 C^1 PH quintic closed loops

We wish to study the construction of spatial PH curves $\mathbf{r}(\xi)$, $\xi \in [\,0, 1\,]$ that form C^1 closed loops, with identical initial and final points $\mathbf{p}_i = \mathbf{p}_f$ and unit tangents $\mathbf{t}_i = \mathbf{t}_f$ at $\xi = 0$ and $\xi = 1$, and a prescribed total arc length S. The construction builds on the analysis developed in [8] — which establishes the existence of a two–parameter family of spatial PH quintic interpolants to given G^1 Hermite data with any prescribed arc length $S > |\mathbf{p}_f - \mathbf{p}_i|$.

3.1 Analysis of the interpolant

We focus here on *canonical form* data specified by $\mathbf{p}_i = \mathbf{p}_f = \mathbf{0}$, $\mathbf{t}_i = \mathbf{t}_f = \mathbf{i}$, and $S = 1$. An arbitrary initial/final point $\mathbf{p}$ can be imposed by choosing it as the integration constant for $\mathbf{r}'(\xi)$, and a general initial/final tangent $\mathbf{t}$ and arc length S can be obtained through a scaling/rotation transformation, achieved by replacing (1) with $\mathcal{A}(\xi)\,\mathcal{Q}$, where $\mathcal{Q}$ is the constant quaternion that satisfies the equation

$$\mathcal{Q}\,\mathbf{i}\,\mathcal{Q}^* = S\,\mathbf{t}\,,$$

whose solutions may be expressed in terms of a free parameter ϕ as

$$\mathcal{Q} = \sqrt{S}\,\frac{\mathbf{t}+\mathbf{i}}{|\,\mathbf{t}+\mathbf{i}\,|}\,\exp(\mathbf{i}\,\phi)\,.$$

Using the Hopf map form defined by (3)–(4), satisfaction of the end–point condition $\mathbf{r}(1) = \mathbf{r}(0) = \mathbf{0}$ yields one real and one complex equation, namely

$$\int_0^1 |\boldsymbol{\alpha}(\xi)|^2 - |\boldsymbol{\beta}(\xi)|^2 \,\mathrm{d}\xi = 0 \quad \text{and} \quad \int_0^1 2\,\boldsymbol{\alpha}(\xi)\overline{\boldsymbol{\beta}}(\xi)\,\mathrm{d}\xi = 0\,, \qquad (8)$$

while imposing the arc length $S = 1$ yields the real equation

$$\int_0^1 |\boldsymbol{\alpha}(\xi)|^2 + |\boldsymbol{\beta}(\xi)|^2\,\mathrm{d}\xi = 1\,. \qquad (9)$$

Combining the first of equations (8) with (9) yields the simpler conditions

$$\int_0^1 |\boldsymbol{\alpha}(\xi)|^2\,\mathrm{d}\xi = \tfrac{1}{2} \quad \text{and} \quad \int_0^1 |\boldsymbol{\beta}(\xi)|^2\,\mathrm{d}\xi = \tfrac{1}{2}\,. \qquad (10)$$

We focus on the spatial PH quintics, which are generated by complex quadratic polynomials expressed in terms of the Bernstein basis

$$b_i^m(\xi) = \binom{m}{i}(1-\xi)^{m-i}\xi^i\,, \quad i = 0,\dots,m$$

on $\xi \in [\,0,1\,]$ as

$$\begin{aligned}
\boldsymbol{\alpha}(\xi) &= \boldsymbol{\alpha}_0\,b_0^2(\xi) + \boldsymbol{\alpha}_1\,b_1^2(\xi) + \boldsymbol{\alpha}_2\,b_2^2(\xi)\,,\\
\boldsymbol{\beta}(\xi) &= \boldsymbol{\beta}_0\,b_0^2(\xi) + \boldsymbol{\beta}_1\,b_1^2(\xi) + \boldsymbol{\beta}_2\,b_2^2(\xi)\,.
\end{aligned} \qquad (11)$$

4

The second of equations (8) then reduces to

$$6\,\boldsymbol{\alpha}_0\overline{\boldsymbol{\beta}}_0 + 3\,\boldsymbol{\alpha}_0\overline{\boldsymbol{\beta}}_1 + 3\,\boldsymbol{\alpha}_1\overline{\boldsymbol{\beta}}_0 + \boldsymbol{\alpha}_0\overline{\boldsymbol{\beta}}_2 + \boldsymbol{\alpha}_2\overline{\boldsymbol{\beta}}_0$$
$$+ 4\,\boldsymbol{\alpha}_1\overline{\boldsymbol{\beta}}_1 + 3\,\boldsymbol{\alpha}_1\overline{\boldsymbol{\beta}}_2 + 3\,\boldsymbol{\alpha}_2\overline{\boldsymbol{\beta}}_1 + 6\,\boldsymbol{\alpha}_2\overline{\boldsymbol{\beta}}_2 \;=\; 0\,, \qquad (12)$$

while equations (10) become

$$6\,|\boldsymbol{\alpha}_0|^2 + 6\,\mathrm{Re}(\boldsymbol{\alpha}_0\overline{\boldsymbol{\alpha}}_1) + 2\,\mathrm{Re}(\boldsymbol{\alpha}_0\overline{\boldsymbol{\alpha}}_2)$$
$$+ 4\,|\boldsymbol{\alpha}_1|^2 + 6\,\mathrm{Re}(\boldsymbol{\alpha}_1\overline{\boldsymbol{\alpha}}_2) + 6\,|\boldsymbol{\alpha}_2|^2 \;=\; 15\,, \qquad (13)$$
$$6\,|\boldsymbol{\beta}_0|^2 + 6\,\mathrm{Re}(\boldsymbol{\beta}_0\overline{\boldsymbol{\beta}}_1) + 2\,\mathrm{Re}(\boldsymbol{\beta}_0\overline{\boldsymbol{\beta}}_2)$$
$$+ 4\,|\boldsymbol{\beta}_1|^2 + 6\,\mathrm{Re}(\boldsymbol{\beta}_1\overline{\boldsymbol{\beta}}_2) + 6\,|\boldsymbol{\beta}_2|^2 \;=\; 15\,. \qquad (14)$$

For C^1 continuity, we assume that $|\mathbf{r}'(0)| = |\mathbf{r}'(1)| = w^2$ where $w > 0$. Then to match the end tangents $(\boldsymbol{\alpha}_0, \boldsymbol{\beta}_0)$ and $(\boldsymbol{\alpha}_2, \boldsymbol{\beta}_2)$ must satisfy

$$\frac{|\boldsymbol{\alpha}_0|^2 - |\boldsymbol{\beta}_0|^2}{|\boldsymbol{\alpha}_0|^2 + |\boldsymbol{\beta}_0|^2} \;=\; \frac{|\boldsymbol{\alpha}_2|^2 - |\boldsymbol{\beta}_2|^2}{|\boldsymbol{\alpha}_2|^2 + |\boldsymbol{\beta}_2|^2} \;=\; 1\,, \qquad \frac{2\,\boldsymbol{\alpha}_0\overline{\boldsymbol{\beta}}_0}{|\boldsymbol{\alpha}_0|^2 + |\boldsymbol{\beta}_0|^2} \;=\; \frac{2\,\boldsymbol{\alpha}_2\overline{\boldsymbol{\beta}}_2}{|\boldsymbol{\alpha}_2|^2 + |\boldsymbol{\beta}_2|^2} \;=\; 0\,,$$

and consequently they must be of the form

$$\boldsymbol{\alpha}_0 \;=\; w\,\exp(\mathrm{i}\,\psi_0)\,, \quad \boldsymbol{\beta}_0 \;=\; 0\,, \quad \boldsymbol{\alpha}_2 \;=\; w\,\exp(\mathrm{i}\,\psi_2)\,, \quad \boldsymbol{\beta}_2 \;=\; 0\,, \qquad (15)$$

where ψ_0 and ψ_2 are free parameters.[3]

Proposition 1. *A canonical–form C^1 PH quintic closed loop $\mathbf{r}(\xi)$ satisfying $|\mathbf{r}'(0)| = |\mathbf{r}'(1)| = w^2$ is uniquely identified in terms of the parameters ψ_0, ψ_2 in* (15) *by the coefficients*

$$\boldsymbol{\alpha}_0 \;=\; w\,\exp(\mathrm{i}\,\psi_0)\,, \quad \boldsymbol{\beta}_0 \;=\; 0\,,$$

$$\boldsymbol{\alpha}_1 \;=\; -\frac{3}{4}\,w\,[\,\exp(\mathrm{i}\,\psi_0) + \exp(\mathrm{i}\,\psi_2)\,]\,, \quad \boldsymbol{\beta}_1 \;=\; \frac{\sqrt{15}}{2}\,,$$

$$\boldsymbol{\alpha}_2 \;=\; w\,\exp(\mathrm{i}\,\psi_2)\,, \quad \boldsymbol{\beta}_2 \;=\; 0\,,$$

where w is specified by

$$w \;=\; \sqrt{\frac{6}{3 - \cos(\psi_2 - \psi_0)}}\,. \qquad (16)$$

---

[3]The parameters ψ_0 and ψ_2 determine the orientation of normal–plane vectors of the Euler–Rodrigues frame at the curve end points, and they also influence the curve shape.

Proof : Using the coefficients (15), equation (12) simplifies to

$$(3\,\boldsymbol{\alpha}_0 + 4\,\boldsymbol{\alpha}_1 + 3\,\boldsymbol{\alpha}_2)\,\overline{\boldsymbol{\beta}}_1 \;=\; 0\,.$$

Discounting the case $\boldsymbol{\beta}_1 = 0$ — in which $\boldsymbol{\beta}(\xi) \equiv 0$, and expression (4) yields a straight line — we must have

$$\boldsymbol{\alpha}_1 \;=\; -\frac{3}{4}\,(\boldsymbol{\alpha}_0 + \boldsymbol{\alpha}_2)\,.$$

Substituting this with $\boldsymbol{\alpha}_0, \boldsymbol{\alpha}_2$ given by (15) into (13) gives (after considerable simplication) the unique value (16) for w — which is obviously real for any choice of ψ_0, ψ_2. Finally, from equation (14) with $\boldsymbol{\beta}_0, \boldsymbol{\beta}_2$ given by (15) we obtain $4\,|\boldsymbol{\beta}_1|^2 = 15$, and hence

$$\boldsymbol{\beta}_1 \;=\; \frac{\sqrt{15}}{2}\,\exp(\mathrm{i}\,\psi_1)\,,$$

where ψ_1 is a free parameter. Since the expression (4) remains unchanged on replacing $\boldsymbol{\alpha}(\xi)$ and $\boldsymbol{\beta}(\xi)$ with $\exp(\mathrm{i}\,\psi)\,\boldsymbol{\alpha}(\xi)$ and $\exp(\mathrm{i}\,\psi)\,\boldsymbol{\beta}(\xi)$ for any ψ, we may choose $\psi_1 = 0$ without loss of generality. ∎

Note that the corresponding coefficients of the quaternion polynomial $\mathcal{A}(\xi) = \mathcal{A}_0\,b_0^2(\xi) + \mathcal{A}_1\,b_1^2(\xi) + \mathcal{A}_2\,b_2^2(\xi)$ in (2) are

$$\mathcal{A}_0 \;=\; w\,(\cos\psi_0 + \sin\psi_0\,\mathbf{i})\,,$$
$$\mathcal{A}_1 \;=\; -\frac{3}{4}\,w\,[\,(\cos\psi_0 + \cos\psi_2) + (\sin\psi_0 + \sin\psi_2)\,\mathbf{i}\,] + \frac{\sqrt{15}}{2}\,\mathbf{k}\,,$$
$$\mathcal{A}_2 \;=\; w\,(\cos\psi_2 + \sin\psi_2\,\mathbf{i})\,.$$

We now present a few examples of C^1 PH quintic closed loops determined by different choices of the parameters ψ_0 and ψ_2.

Example 1. Consider the case $\psi_2 = \psi_0 + \pi/2$, so that $w = \sqrt{2}$. Figure 1 illustrates the family of C^1 PH quintic closed loops determined by $\psi_0 = k\pi/30$ for $0 \leq k \leq 20$ and $\psi_2 = \psi_0 + \pi/2$, with hue values varying from red to blue.

Remark 1. When $\psi_2 = \psi_0 + k\pi$ for even k, we have $w = \sqrt{3}$ and hence

$$u(\xi) \;=\; \sqrt{3}\,\cos\psi_0\,[\,1 - \frac{5}{2}\,b_1^2(\xi)\,]\,, \quad v(\xi) \;=\; \sqrt{3}\,\sin\psi_0\,[\,1 - \frac{5}{2}\,b_1^2(\xi)\,]\,,$$
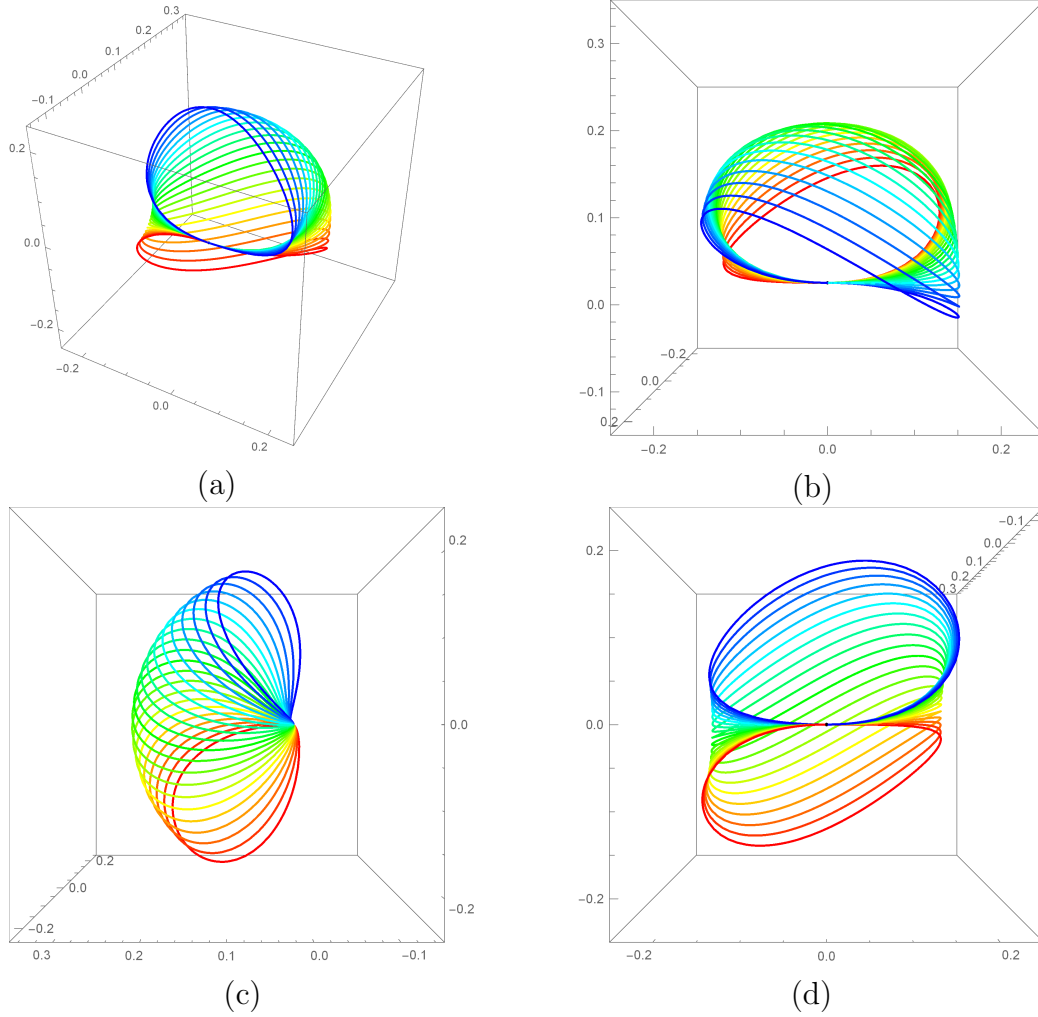
6

Figure 1: The family of C^1 PH quintic closed loops determined by $\psi_0 = k\pi/30$ for $0 \le k \le 20$ and $\psi_2 = \psi_0 + \pi/2$ are shown with hues varying from red to blue and different viewpoints — (a) perspective, (b) top, (c) left, (d) front.

$$p(\xi) \;=\; 0\,, \quad q(\xi) \;=\; \frac{\sqrt{15}}{2}\, b_1^2(\xi)\,,$$

and by the partition–of–unity property of the Bernstein basis, we obtain

$$x'(\xi) \;=\; 3\,[\,1 - \tfrac{5}{2}\,b_1^2(\xi)\,]^2 - \frac{15}{4}\,[\,b_1^2(\xi)\,]^2\,,$$

$$y'(\xi) \;=\; 3\sqrt{5}\,\cos\psi_0\,[\,1 - \tfrac{5}{2}\,b_1^2(\xi)\,]\,b_1^2(\xi)\,,$$

$$z'(\xi) \;=\; 3\sqrt{5}\,\sin\psi_0\,[\,1 - \tfrac{5}{2}\,b_1^2(\xi)\,]\,b_1^2(\xi)\,.$$

When $\psi_2 = \psi_0 + k\pi$ for odd k, on the other hand, we have $w = \sqrt{6}/2$ and hence

$$u(\xi) \;=\; \frac{\sqrt{6}}{2}\,\cos\psi_0\,[\,b_0^2(\xi) - b_2^2(\xi)\,]\,, \quad v(\xi) \;=\; \frac{\sqrt{6}}{2}\,\sin\psi_0\,[\,b_0^2(\xi) - b_2^2(\xi)\,]\,,$$

$$p(\xi) \;=\; 0\,, \quad q(\xi) \;=\; \frac{\sqrt{15}}{2}\, b_1^2(\xi)\,.$$

Consequently,

$$x'(\xi) \;=\; \frac{3}{2}\,[\,b_0^2(\xi) - b_2^2(\xi)\,]^2 - \frac{15}{4}\,[\,b_1^2(\xi)\,]^2\,,$$

$$y'(\xi) \;=\; \frac{3\sqrt{10}}{2}\,\cos\psi_0\,[\,b_0^2(\xi) - b_2^2(\xi)\,]\,b_1^2(\xi)\,,$$

$$z'(\xi) \;=\; \frac{3\sqrt{10}}{2}\,\sin\psi_0\,[\,b_0^2(\xi) - b_2^2(\xi)\,]\,b_1^2(\xi)\,.$$

In both cases, $y'(\xi)$ and $z'(\xi)$ are linearly dependent, and we have $\mathbf{n}\cdot\mathbf{r}'(\xi) \equiv 0$ where $\mathbf{n} = (0, \sin\psi_0, -\cos\psi_0)$. The curve lies in the plane through the origin defined in terms of coordinates $\mathbf{p} = (x, y, z)$ by $\mathbf{n}\cdot\mathbf{p} = 0$. For $0 \le \psi_0 < 2\pi$, these planes form a pencil about the x–axis as a common line.

Example 2. For the choice $\psi_0 = k\pi/10$ with $0 \le k \le 5$, Figure 2 illustrates the family of planar C^1 PH quintic closed loops together with the pencil of the planes when $\psi_2 = \psi_0$, while Figure 3 illustrates the family of curves and pencil of the planes when $\psi_2 = \psi_0 + \pi$.

3.2   Control points of the interpolant

The control points $\mathbf{p}_0, \ldots, \mathbf{p}_5$ for the Bézier representation

$$\mathbf{r}(\xi) \;=\; \sum_{i=0}^{5} \mathbf{p}_i\, b_i^5(\xi)$$
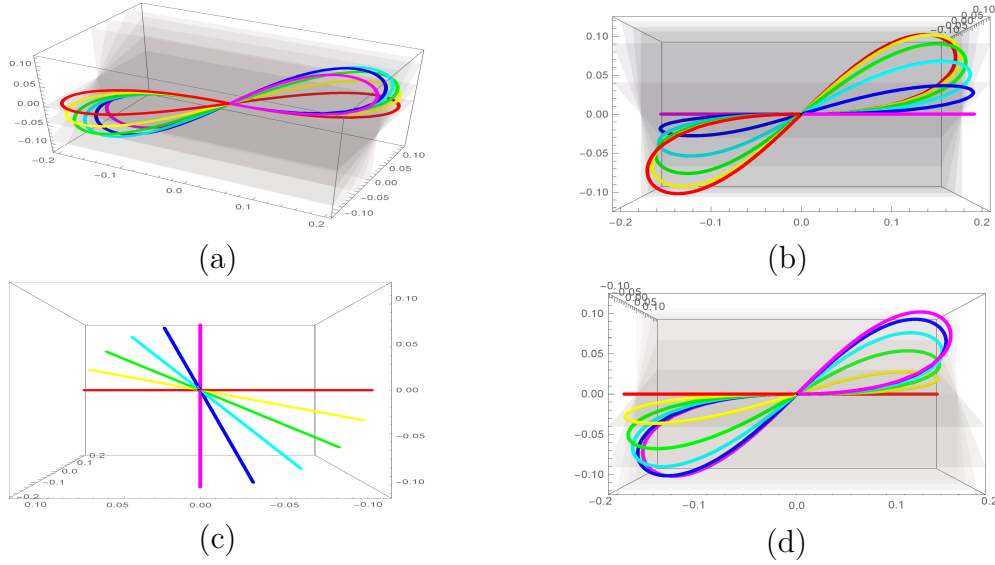
8

Figure 2: The family of C^1 PH quintic closed loops determined by $\psi_0 = k\pi/10$ for $0 \le k \le 5$ and $\psi_2 = \psi_0$ are shown together with the pencil of the planes from different viewpoints — (a) perspective, (b) top, (c) left, (d) front.
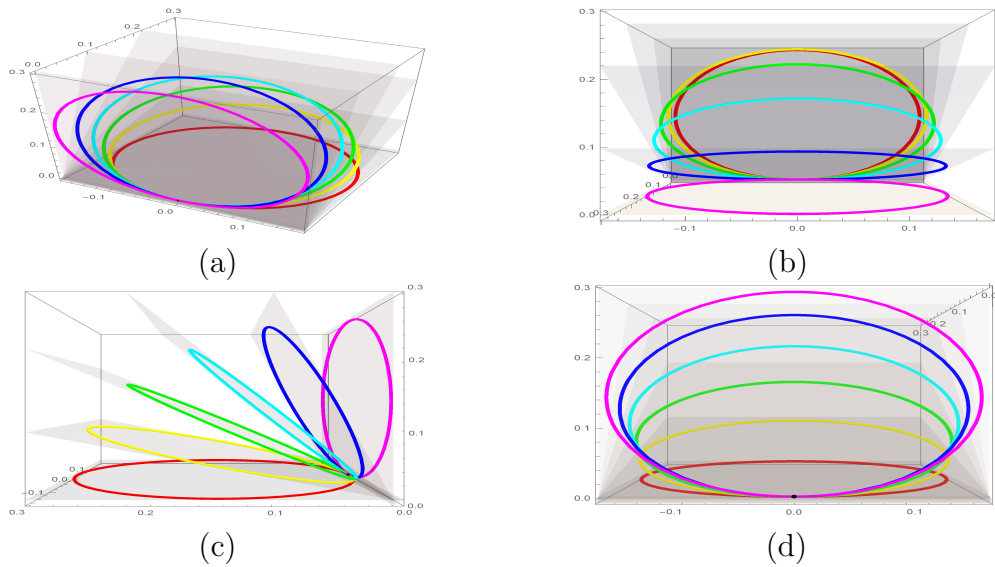

Figure 3: The family of C^1 PH quintic closed loops determined by $\psi_0 = k\pi/10$ for $0 \le k \le 5$ and $\psi_2 = \psi_0 + \pi$ are shown together with the pencil of the planes from different viewpoints — (a) perspective, (b) top, (c) left, (d) front.

9

of $\mathbf{r}(\xi)$ may be obtained [5] with integration constant $\mathbf{p}_0 = \mathbf{0}$ as

$$
\begin{aligned}
\mathbf{p}_1 &= \mathbf{p}_0 + \frac{1}{5}\mathcal{A}_0\,\mathbf{i}\,\mathcal{A}_0^*, \\
\mathbf{p}_2 &= \mathbf{p}_1 + \frac{1}{10}(\mathcal{A}_0\,\mathbf{i}\,\mathcal{A}_1^* + \mathcal{A}_1\,\mathbf{i}\,\mathcal{A}_0^*), \\
\mathbf{p}_3 &= \mathbf{p}_2 + \frac{1}{30}(\mathcal{A}_0\,\mathbf{i}\,\mathcal{A}_2^* + 4\,\mathcal{A}_1\,\mathbf{i}\,\mathcal{A}_1^* + \mathcal{A}_2\,\mathbf{i}\,\mathcal{A}_0^*), \\
\mathbf{p}_4 &= \mathbf{p}_3 + \frac{1}{10}(\mathcal{A}_1\,\mathbf{i}\,\mathcal{A}_2^* + \mathcal{A}_2\,\mathbf{i}\,\mathcal{A}_1^*), \\
\mathbf{p}_5 &= \mathbf{p}_4 + \frac{1}{5}\mathcal{A}_2\,\mathbf{i}\,\mathcal{A}_2^*.
\end{aligned}
$$

They may be expressed explicitly in terms of the quantities w, ψ_0, ψ_2 as

$$
\begin{aligned}
\mathbf{p}_0 &= \mathbf{0}, \quad \mathbf{p}_1 = \frac{w^2}{5}\,\mathbf{i}, \\
\mathbf{p}_2 &= \frac{w^2}{20}\,[\,1 - 3\cos(\psi_2 - \psi_0)\,]\,\mathbf{i} + \frac{\sqrt{15}}{10}\,w\,(\cos\psi_0\,\mathbf{j} + \sin\psi_0\,\mathbf{k}), \\
\mathbf{p}_3 &= \frac{w^2}{20}\,[\,3\cos(\psi_2 - \psi_0) - 1\,]\,\mathbf{i} - \frac{\sqrt{15}}{10}\,w\,(\cos\psi_2\,\mathbf{j} + \sin\psi_2\,\mathbf{k}), \\
\mathbf{p}_4 &= -\frac{w^2}{5}\,\mathbf{i}, \quad \mathbf{p}_5 = \mathbf{0}.
\end{aligned}
\tag{17}
$$

If $\psi_2 = \psi_0 + k\pi$ for integer k, the control points satisfy the planarity condition $\mathbf{n} \cdot \mathbf{p}_i = 0$ for $i = 0, \ldots, 5$ where $\mathbf{n} = (0, \sin\psi_0, -\cos\psi_0)$ as in Remark 1.

From (17) we see that the curve $\mathbf{r}(\xi)$ depends *individually* on ψ_0, ψ_2 and not just on their difference. Hence, the problem of constructing a canonical–form C^1 spatial PH quintic loop admits a two–parameter family of solutions.

Remark 2. The ability to construct non–planar C^1 closed loops from single PH quintic segments is a remarkable property. PH quintics are analogous to "ordinary" cubic curves in their shape freedoms [5] — they are the lowest–order curves, in their respective classes, that can match first–order Hermite data. However, an ordinary cubic that satisfies $\mathbf{r}(1) = \mathbf{r}(0)$ and $\mathbf{r}'(1) = \mathbf{r}'(0)$ has colinear Bézier control points $\mathbf{p}_0, \mathbf{p}_1, \mathbf{p}_2, \mathbf{p}_3$ and therefore degenerates to a (multiply–traced) straight line. On the other hand, the quintic PH curves generate true spatial C^1 closed loops of any desired arc length S, and they also incorporate two free shape parameters.

The parametric speed $\sigma(\xi) = |\mathbf{r}'(\xi)|$ is the quartic polynomial specified

by the Bernstein coefficients

$$
\begin{aligned}
\sigma_0 &= |\mathcal{A}_0|^2 = w^2\,, \\
\sigma_1 &= \mathrm{scal}(\mathcal{A}_0\mathcal{A}_1^*) = -\frac{3}{4}\,[\,1 + \cos(\psi_2 - \psi_0)\,]\,w^2\,, \\
\sigma_2 &= \frac{2\,|\mathcal{A}_1|^2 + \mathrm{scal}(\mathcal{A}_2\mathcal{A}_0^*)}{3} = \frac{[\,9 + 13\,\cos(\psi_2 - \psi_0)\,]\,w^2 + 30}{12}\,, \\
\sigma_3 &= \mathrm{scal}(\mathcal{A}_1\mathcal{A}_2^*) = -\frac{3}{4}\,[\,1 + \cos(\psi_2 - \psi_0)\,]\,w^2\,, \\
\sigma_4 &= |\mathcal{A}_2|^2 = w^2\,,
\end{aligned}
\tag{18}
$$

and the corresponding polynomial arc length function

$$
s(\xi) = \int_0^\xi \sigma(t)\,\mathrm{d}t = \sum_{i=0}^5 s_i\,b_i^5(\xi)
\tag{19}
$$

is characterized by the coefficients

$$
s_0 = 0 \quad \text{and} \quad s_i = s_{i-1} + \frac{\sigma_{i-1}}{5}\,, \quad i = 1,\ldots,5\,.
\tag{20}
$$

3.3 Frenet frame, curvature, torsion

For the canonical–form C^1 PH quintic closed loop $\mathbf{r}(\xi)$ we have

$$
u(\xi) = w\cos\psi_0\,b_0^2(\xi) - \frac{3}{4}\,w\,(\cos\psi_0 + \cos\psi_2)\,b_1^2(\xi) + w\cos\psi_2\,b_2^2(\xi)\,,
$$

$$
v(\xi) = w\sin\psi_0\,b_0^2(\xi) - \frac{3}{4}\,w\,(\sin\psi_0 + \sin\psi_2)\,b_1^2(\xi) + w\sin\psi_2\,b_2^2(\xi)\,,
$$

$$
p(\xi) = 0\,, \quad q(\xi) = \frac{\sqrt{15}}{2}\,b_1^2(\xi)\,.
$$

The Frenet frame $(\mathbf{t}(\xi), \mathbf{n}(\xi), \mathbf{b}(\xi))$ and the curvature $\kappa(\xi)$ and torsion $\tau(\xi)$ of $\mathbf{r}(\xi)$ are defined [20] by

$$
\mathbf{t}(\xi) = \frac{\mathbf{r}'(\xi)}{|\mathbf{r}'(\xi)|}\,, \quad \mathbf{n}(\xi) = \frac{\mathbf{r}'(\xi) \times \mathbf{r}''(\xi)}{|\mathbf{r}'(\xi) \times \mathbf{r}''(\xi)|} \times \mathbf{t}(\xi)\,, \quad \mathbf{b}(\xi) = \frac{\mathbf{r}'(\xi) \times \mathbf{r}''(\xi)}{|\mathbf{r}'(\xi) \times \mathbf{r}''(\xi)|}\,,
$$

$$
\kappa(\xi) = \frac{|\mathbf{r}'(\xi) \times \mathbf{r}''(\xi)|}{\sigma^3(\xi)}\,, \quad \tau(\xi) = \frac{(\mathbf{r}'(\xi) \times \mathbf{r}''(\xi)) \cdot \mathbf{r}'''(\xi)}{|\mathbf{r}'(\xi) \times \mathbf{r}''(\xi)|^2}\,.
$$

11

Now every spatial PH curve satisfies [13] the relation

$$|\mathbf{r}'(\xi) \times \mathbf{r}''(\xi)|^2 \;=\; 4\,\sigma^2(\xi)\,\rho(\xi)\,,$$

where $\rho(\xi)$ is the polynomial defined by

$$\rho \;=\; (up' - u'p + vq' - v'q)^2 + (uq' - u'q - vp' + v'p)^2\,. \tag{21}$$

Using `Maple` we find that, for the canonical–form C^1 closed–loop PH quintic, the quartic polynomial $\rho(\xi)$ has the symmetric Bernstein coefficients

$$\rho_0 = \rho_4 = 15\,w^2\,, \quad \rho_1 = \rho_3 = 0\,, \quad \rho_2 = -\,5\,w^2\cos(\psi_2 - \psi_0)\,, \tag{22}$$

and for the scalar triple product $f(\xi) = (\mathbf{r}'(\xi) \times \mathbf{r}''(\xi)) \cdot \mathbf{r}'''(\xi)$ we obtain the degree 6 polynomial

$$f(\xi) \;=\; w^2 \sin(\psi_0 - \psi_2) \sum_{i=0}^{6} f_i\, b_i^6(\xi) \tag{23}$$

with the symmetric Bernstein coefficients

$$f_0 = f_6 = 180\,w^2\,, \quad f_1 = f_5 = -\,60\,w^2\,, \quad f_2 = f_4 = 36\,w^2\,,$$

$$f_3 = -\,[\,27 + 15\cos(\psi_2 - \psi_0)\,]\,w^2 - 90\,. \tag{24}$$

Hence, the curvature and torsion can be written as

$$\kappa(\xi) \;=\; \frac{2\,\sqrt{\rho(\xi)}}{\sigma^2(\xi)}\,, \quad \tau(\xi) \;=\; \frac{f(\xi)}{4\,\sigma^2(\xi)\,\rho(\xi)}\,. \tag{25}$$

The form (23) indicates that $\mathbf{r}(\xi)$ degenerates to a planar curve if ψ_0 and ψ_2 differ by an integer multiple of π, consistent with Remark 1.

Remark 3. Although the PH quintic closed loop was constructed with only C^1 continuity at the point $\mathbf{r}(1) = \mathbf{r}(0)$, we note from expressions (25) and the coefficients (18) of the parametric speed, and from (21)–(22) and (23)–(24), that $\kappa(1) = \kappa(0) = 2\sqrt{15}/w^2$ and $\tau(1) = \tau(0) = -\,3/w^2$, so $\mathbf{r}(\xi)$ is actually continuous in *tangent*, *curvature*, and *torsion* at $\mathbf{r}(0) = \mathbf{r}(1)$. The normal and binormal are not continuous, however, since

$$\mathbf{n}(0) \;=\; (0, \cos\psi_0, \sin\psi_0)\,, \quad \mathbf{n}(1) \;=\; (0, -\cos\psi_2, -\sin\psi_2)\,,$$

$$\mathbf{b}(0) \;=\; (0, -\sin\psi_0, \cos\psi_0)\,, \quad \mathbf{b}(1) \;=\; (0, \sin\psi_2, -\cos\psi_2)\,.$$

3.4 Twist of the Euler–Rodrigues frame

We now consider the behavior of the ERF along the canonical C^1 PH quintic closed loop $\mathbf{r}(\xi)$.

Lemma 1. *For the canonical–form C^1 PH quintic closed loop, the tangent component (6) of the ERF angular velocity cannot change sign.*

Proof : Since $\sigma(\xi) = u^2(\xi) + v^2(\xi) + p^2(\xi) + q^2(\xi) > 0$ for all ξ, expression (6) for $\omega_1(\xi)$ can only change sign if $h(\xi)$ defined by (7) changes sign. However, using the above forms for $u(\xi), v(\xi), p(\xi), q(\xi)$ the polynomial (7) reduces to the quadratic expression

$$h(\xi) \;=\; \frac{1}{2}\, w^2 \sin(\psi_0 - \psi_2)\, [\, 3\, b_0^2(\xi) - 2\, b_1^2(\xi) + 3\, b_2^2(\xi) \,]. \tag{26}$$

Since $h(\xi)$ has a negative discriminant, it has no roots on $[\,0,1\,]$ and $\omega_1(\xi)$ can not change sign on this interval. ∎

Hence, the normal–plane vectors $\mathbf{e}_2(\xi), \mathbf{e}_3(\xi)$ maintain a consistent sense of rotation about the tangent $\mathbf{e}_1(\xi)$. This eliminates the need to consider the possibility of *inflections* (reversals in the sense of rotation) of the ERF — as was necessary in [15] for the case of general PH quintic space curves.

The *twist* T_{ERF} of the ERF characterizes the total rotation of the normal–plane vectors $\mathbf{e}_2, \mathbf{e}_3$ about the tangent $\mathbf{e}_1$ along $\mathbf{r}(\xi)$, namely

$$T_{\mathrm{ERF}} \;=\; \int_0^S \omega_1 \, \mathrm{d}s \;=\; \int_0^1 \omega_1(\xi)\, \sigma(\xi)\, \mathrm{d}\xi \;=\; 2 \int_0^1 \frac{h(\xi)}{\sigma(\xi)} \, \mathrm{d}\xi \,. \tag{27}$$

As noted in Lemma 1, the integrand in the above expression cannot change sign. This integrand has a numerator of degree 2 and denominator of degree 4, and the integral admits closed–form reduction through a partial fraction decomposition. Let $\mathbf{z}_1, \bar{\mathbf{z}}_1$ and $\mathbf{z}_2, \bar{\mathbf{z}}_2$ be the two pairs of complex conjugate roots[4] of $\sigma(\xi) = u^2(\xi) + v^2(\xi) + p^2(\xi) + q^2(\xi)$, so that

$$\sigma(\xi) \;=\; c\,(\xi - \mathbf{z}_1)(\xi - \bar{\mathbf{z}}_1)(\xi - \mathbf{z}_2)(\xi - \bar{\mathbf{z}}_2)$$

for some real constant $c \neq 0$. A closed–form solution for the roots is possible using Ferrari's method [22]. Dividing $h(\xi)$ and $\sigma(\xi)$ by c, the partial–fraction decomposition of the integrand in (27) has the form

$$\frac{h(\xi)}{\sigma(\xi)} \;=\; \frac{\mathbf{c}_1}{\xi - \mathbf{z}_1} + \frac{\bar{\mathbf{c}}_1}{\xi - \bar{\mathbf{z}}_1} + \frac{\mathbf{c}_2}{\xi - \mathbf{z}_2} + \frac{\bar{\mathbf{c}}_2}{\xi - \bar{\mathbf{z}}_2} \,, \tag{28}$$

---

[4]Because of the symmetry of the coefficients (18), the roots of $\sigma(\xi)$ are symmetrically disposed about the interval $[\,0,1\,]$ — they are of the form $a \pm \mathrm{i}\,b$ and $1 - a \pm \mathrm{i}\,b$ for real a, b.

where the complex values

$$\mathbf{c}_1 \;=\; \frac{h(\mathbf{z}_1)}{(\mathbf{z}_1 - \overline{\mathbf{z}}_1)(\mathbf{z}_1 - \mathbf{z}_2)(\mathbf{z}_1 - \overline{\mathbf{z}}_2)}\,, \quad \mathbf{c}_2 \;=\; \frac{h(\mathbf{z}_2)}{(\mathbf{z}_2 - \mathbf{z}_1)(\mathbf{z}_2 - \overline{\mathbf{z}}_1)(\mathbf{z}_2 - \overline{\mathbf{z}}_2)} \quad (29)$$

are the *residues* of $h(\xi)/\sigma(\xi)$ at its poles $\mathbf{z}_1, \mathbf{z}_2$ and $\overline{\mathbf{c}}_1, \overline{\mathbf{c}}_2$ are their conjugates. From (28) we then have the indefinite integral

$$\int \frac{h(\xi)}{\sigma(\xi)}\,\mathrm{d}\xi \;=\; \mathbf{c}_1 \ln(\xi - \mathbf{z}_1) + \overline{\mathbf{c}}_1 \ln(\xi - \overline{\mathbf{z}}_1)$$
$$+\; \mathbf{c}_2 \ln(\xi - \mathbf{z}_2) + \overline{\mathbf{c}}_2 \ln(\xi - \overline{\mathbf{z}}_2)\,, \quad (30)$$

and by combining conjugate terms we obtain the real expression

$$\int \frac{h(\xi)}{\sigma(\xi)}\,\mathrm{d}\xi \;=\; 2\operatorname{Re}(\mathbf{c}_1) \ln|\xi - \mathbf{z}_1| - 2\operatorname{Im}(\mathbf{c}_1) \arg(\xi - \mathbf{z}_1)$$
$$+\; 2\operatorname{Re}(\mathbf{c}_2) \ln|\xi - \mathbf{z}_2| - 2\operatorname{Im}(\mathbf{c}_2) \arg(\xi - \mathbf{z}_2)\,. \quad (31)$$

T_{ERF} is obtained by evaluating (31) between the limits $\xi = 0$ and $\xi = 1$.

3.5 Representative examples

We now present a few examples of the C^1 PH quintic closed loops, which will subsequently be used as reference curves for the frame construction problem.

Example 3. For the canonical–form loop corresponding to parameter values $\psi_0 = 0$ and $\psi_2 = \pi/2$ we obtain $w = \sqrt{2}$ from (16). With $\mathbf{p}_0 = \mathbf{p}_5 = (0, 0, 0)$ the interior control points are

$$\mathbf{p}_1 \;=\; (2/5, 0, 0)\,, \quad \mathbf{p}_2 \;=\; (1/10, \sqrt{30}/10, 0)\,,$$
$$\mathbf{p}_3 \;=\; (-1/10, 0, -\sqrt{30}/10)\,, \quad \mathbf{p}_4 \;=\; (-2/5, 0, 0)\,,$$

and for the coefficients (18) of the parametric speed we obtain

$$(\sigma_0, \sigma_1, \sigma_2, \sigma_3, \sigma_4) \;=\; (2, -3/2, 4, -3/2, 2)\,.$$

The roots of $\sigma(\xi)$ are $0.158596 \pm 0.203855\,\mathrm{i}$ and $0.841404 \pm 0.203855\,\mathrm{i}$, and the quadratic polynomial (7) has coefficients

$$(h_0, h_1, h_2) \;=\; (-3, 2, -3)\,.$$

Hence, we obtain the ERF twist from (27), (29), and (31) as

$$T_{\mathrm{ERF}} \;=\; -2.613462\,.$$

Figure 4 illustrates this curve together with the ERF normal–plane vectors, and Figure 5 shows its curvature and torsion profiles.
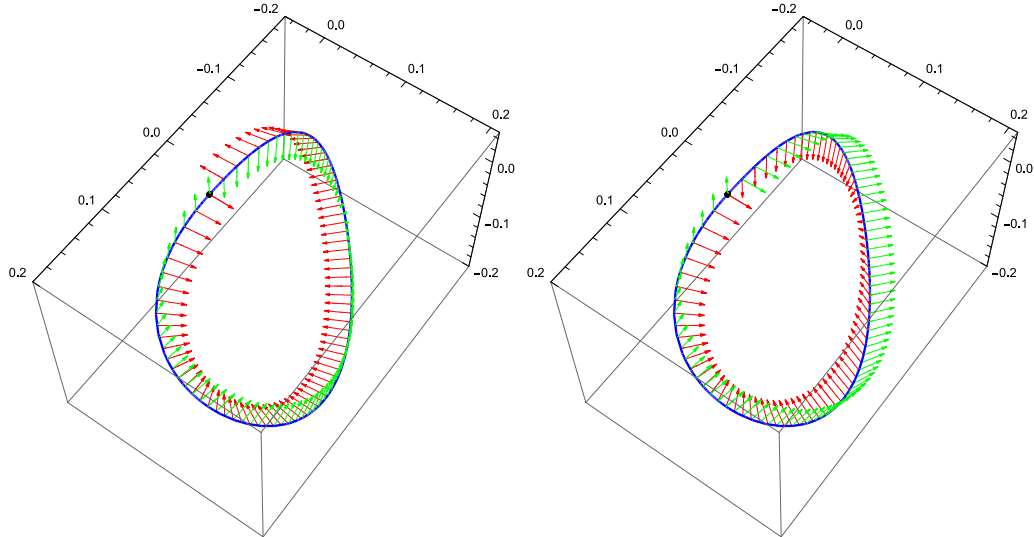
14

Figure 4: The C^1 PH quintic closed loop constructed in Example 1, showing the normal–plane vectors of (left) the Euler–Rodrigues frame and (right) the Frenet frame. Note the mismatch of the normal–plane vectors for both these frames at the C^1 loop juncture point $\mathbf{r}(0) = \mathbf{r}(1)$, identified by a dot.
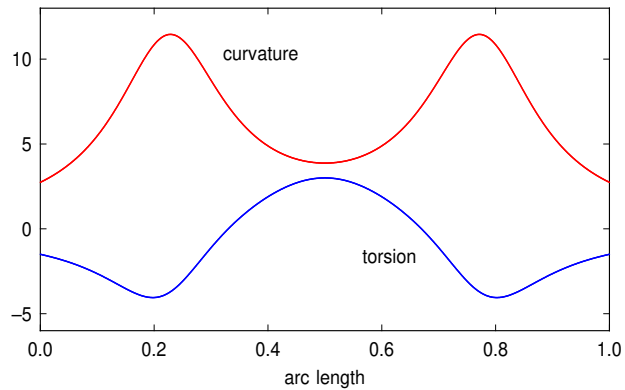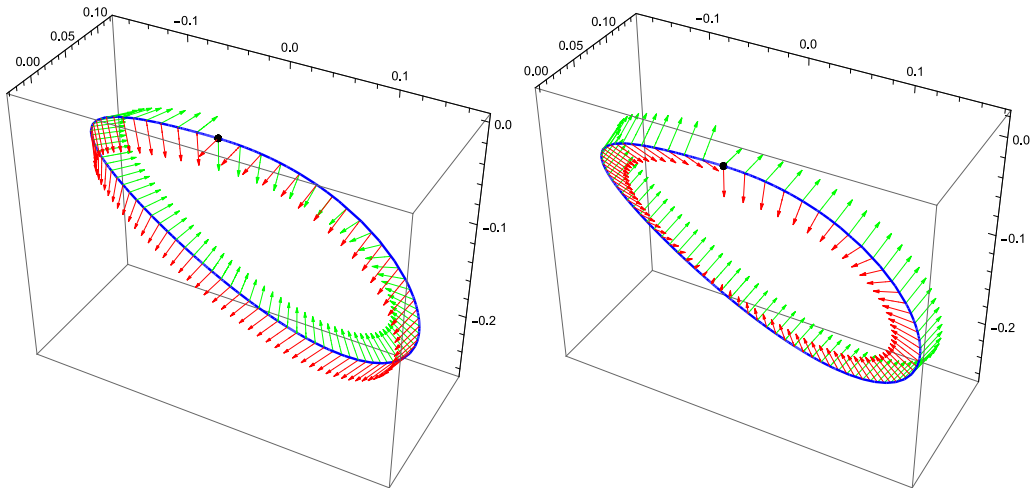

Figure 5: Curvature and torsion profiles for the canonical–form C^1 closed loop in Example 1, specified by the parameter values $\psi_0 = 0$ and $\psi_2 = \pi/2$.

15

Example 4. For the canonical–form loop corresponding to parameter values $\psi_0 = -\pi/2$ and $\psi_2 = 3\pi/4$ we obtain

$$w = \left[\frac{6\sqrt{2}}{3\sqrt{2}+1} \right]^{1/2} .$$

In this case, the ERF twist is

$$T_{\mathrm{ERF}} = 1.464840 .$$

As seen in Figures 6 and 7, the curve has a milder deviation from planarity than the curve in Example 3.

Figure 6: The C^1 PH quintic closed loop constructed in Example 2, showing the normal–plane vectors of (left) the Euler–Rodrigues frame and (right) the Frenet frame. Note the mismatch of the normal–plane vectors for both these frames at the C^1 loop juncture point $\mathbf{r}(0) = \mathbf{r}(1)$, identified by a dot.

4   Periodic frames on closed curves

We now address the problem of constructing periodic adapted frames along space curves that form closed loops.
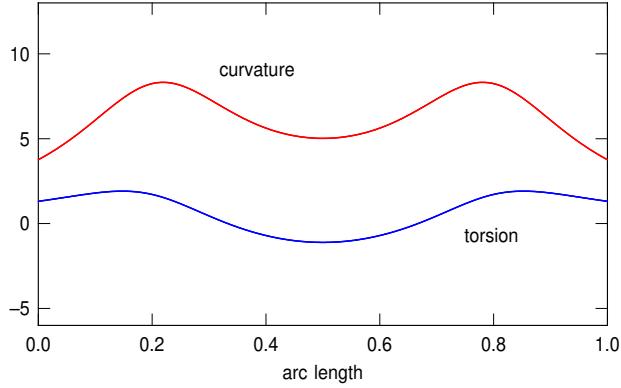
16

Figure 7: Curvature and torsion profiles for the canonical–form C^1 closed loop in Example 2, specified by the parameter values $\psi_0 = -\frac{1}{2}\pi$ and $\psi_2 = \frac{3}{4}\pi$.

4.1 Phase angle between adapted frames

We first introduce the concept of the phase angle between two adapted frames $(\mathbf{f}_1(\xi), \mathbf{f}_2(\xi), \mathbf{f}_3(\xi))$ and $(\mathbf{g}_1(\xi), \mathbf{g}_2(\xi), \mathbf{g}_3(\xi))$ along a given space curve $\mathbf{r}(\xi)$. It is assumed herein that all adapted frames are positively oriented, in the sense that $\mathbf{f}_1 \times \mathbf{f}_2 = \mathbf{f}_3$.

Definition 1. *Let $(\mathbf{f}_1, \mathbf{f}_2, \mathbf{f}_3)$ and $(\mathbf{g}_1, \mathbf{g}_2, \mathbf{g}_3)$ be adapted frames along the space curve $\mathbf{r}(\xi)$. Then the* phase angle *$\theta(\xi)$ of $(\mathbf{g}_1, \mathbf{g}_2, \mathbf{g}_3)$ relative to $(\mathbf{f}_1, \mathbf{f}_2, \mathbf{f}_3)$ is a real–valued function such that*

$$\left[\begin{array}{c} \mathbf{g}_2(\xi) \\ \mathbf{g}_3(\xi) \end{array} \right] = \left[\begin{array}{cc} \cos\theta(\xi) & \sin\theta(\xi) \\ -\sin\theta(\xi) & \cos\theta(\xi) \end{array} \right] \left[\begin{array}{c} \mathbf{f}_2(\xi) \\ \mathbf{f}_3(\xi) \end{array} \right] . \tag{32}$$

The phase angle $\theta(\xi)$ is evidently a continuous function if $(\mathbf{f}_1, \mathbf{f}_2, \mathbf{f}_3)$ and $(\mathbf{g}_1, \mathbf{g}_2, \mathbf{g}_3)$ are both continuous adapted frames. However, it is indeterminate up to an integer multiple of 2π — i.e., if $\theta(\xi)$ is a phase angle of $(\mathbf{g}_1, \mathbf{g}_2, \mathbf{g}_3)$ relative to $(\mathbf{f}_1, \mathbf{f}_2, \mathbf{f}_3)$ then $\widetilde{\theta}(\xi) = \theta(\xi) + 2k\pi$ for $k \in \mathbb{Z}$ is also a phase angle. So we can always choose $\theta(\xi)$ such that $0 \leq \theta(0) < 2\pi$. Note that the range of the phase angle $\theta(\xi)$ is *not* restricted to $[0, 2\pi)$.

An important instance of the phase angle concerns the orientation of an RMF relative to the Frenet frame. An RMF $(\mathbf{t}, \mathbf{u}, \mathbf{v})$ is characterized by the property that its angular velocity

$$\boldsymbol{\Omega} = \alpha\,\mathbf{t} + \beta\,\mathbf{u} + \gamma\,\mathbf{v}$$

has a vanishing component in the direction of the curve tangent $\mathbf{t}$, i.e., $\alpha \equiv 0$, so the angular velocity has the form[5]

$$\boldsymbol{\Omega} \;=\; -\,(\dot{\mathbf{t}} \cdot \mathbf{v})\,\mathbf{u} + (\dot{\mathbf{t}} \cdot \mathbf{u})\,\mathbf{v}\,.$$

Klok [19] showed that the RMF normal–pane vectors $\mathbf{u}$ and $\mathbf{v}$ are solutions of the system of ordinary differential equations

$$\mathbf{u}'(\xi) \;=\; -\frac{\mathbf{r}''(\xi) \cdot \mathbf{u}(\xi)}{|\mathbf{r}'(\xi)|^2}\,\mathbf{r}'(\xi)\,, \quad \mathbf{v}'(\xi) \;=\; -\frac{\mathbf{r}''(\xi) \cdot \mathbf{v}(\xi)}{|\mathbf{r}'(\xi)|^2}\,\mathbf{r}'(\xi)\,,$$

for given initial conditions $\mathbf{u}(0)$ and $\mathbf{v}(0)$. It is known [18] that the phase angle $\phi(\xi)$ of the RMF relative to the Frenet frame is

$$\phi(\xi) \;=\; \phi_0 - \int_o^\xi \tau(t)\sigma(t)\,\mathrm{d}t\,, \tag{33}$$

where $\tau(\xi)$ and $\sigma(\xi)$ are the torsion and parametric speed of $\mathbf{r}(\xi)$, and ϕ_0 is the phase angle of the initial RMF $(\mathbf{t}(0), \mathbf{u}(0), \mathbf{v}(0))$ relative to the initial Frenet frame $(\mathbf{t}(0), \mathbf{n}(0), \mathbf{b}(0))$.

The following Lemma describes the relation between the angular velocities of two adapted frames on a space curve, in terms of the phase angle between them. This relation has been presented in [15] in the particular context of the MTF and ERF — we state it here for general adapted frames.

Lemma 2. *Let $(\mathbf{f}_1, \mathbf{f}_2, \mathbf{f}_3)$ and $(\mathbf{g}_1, \mathbf{g}_2, \mathbf{g}_3)$ be adapted frames along a space curve $\mathbf{r}(\xi)$, $\xi \in [\,0, 1\,]$ and let $\boldsymbol{\Omega}_\mathbf{f}$ and $\boldsymbol{\Omega}_\mathbf{g}$ be their angular velocities. Then if $\theta(\xi)$ is the phase angle of $(\mathbf{g}_1, \mathbf{g}_2, \mathbf{g}_3)$ with respect to $(\mathbf{f}_1, \mathbf{f}_2, \mathbf{f}_3)$, we have*

$$\boldsymbol{\Omega}_\mathbf{g} \;=\; \boldsymbol{\Omega}_\mathbf{f} + \dot{\theta}\,\mathbf{f}_1 \;=\; \boldsymbol{\Omega}_\mathbf{f} + \frac{\theta'}{\sigma}\,\mathbf{f}_1\,.$$

Proof : We can express the frame angular velocities as

$$\boldsymbol{\Omega}_\mathbf{f} \;=\; \Omega_{\mathbf{f},1}\mathbf{f}_1 + \Omega_{\mathbf{f},2}\mathbf{f}_2 + \Omega_{\mathbf{f},3}\mathbf{f}_3\,, \quad \boldsymbol{\Omega}_\mathbf{g} \;=\; \Omega_{\mathbf{g},1}\mathbf{g}_1 + \Omega_{\mathbf{g},2}\mathbf{g}_2 + \Omega_{\mathbf{g},3}\mathbf{g}_3\,. \tag{34}$$

By straightforward computation using (32), and observing that $\mathbf{f}_i \cdot \dot{\mathbf{f}}_i = 0$ and $\mathbf{f}_j \cdot \dot{\mathbf{f}}_k + \dot{\mathbf{f}}_j \cdot \mathbf{f}_k = 0$, we have

$$\begin{aligned} \Omega_{\mathbf{g},1} = \dot{\mathbf{g}}_2 \cdot \mathbf{g}_3 &= \Omega_{\mathbf{f},1} + \dot{\theta}\,, \\ \Omega_{\mathbf{g},2} = \dot{\mathbf{g}}_3 \cdot \mathbf{g}_1 &= \cos\theta\,\Omega_{\mathbf{f},2} + \sin\theta\,\Omega_{\mathbf{f},3}\,, \\ \Omega_{\mathbf{g},3} = \dot{\mathbf{g}}_1 \cdot \mathbf{g}_2 &= -\sin\theta\,\Omega_{\mathbf{f},2} + \cos\theta\,\Omega_{\mathbf{f},3}\,. \end{aligned}$$

---

[5]Here dots denote derivatives with respect to the curve arc length s.

Substituting these expressions and (32) into (34) then yields

$$\boldsymbol{\Omega_g} \;=\; \boldsymbol{\Omega_f} + \dot\theta\, \mathbf{f}_1\,. \qquad\blacksquare$$

For adapted frames, the first component of the angular velocity plays an important role, since it determines the rate of rotation of the normal–plane vectors. If two frames $(\mathbf{f}_1, \mathbf{f}_2, \mathbf{f}_3)$ and $(\mathbf{g}_1, \mathbf{g}_2, \mathbf{g}_3)$ are as in Lemma 2, their angular velocity components in the direction $\mathbf{f}_1 = \mathbf{g}_1$ satisfy

$$\Omega_{\mathbf{g},1} \;=\; \Omega_{\mathbf{f},1} + \dot\theta\,,$$

and consequently their twists $T_{\mathbf{f}}$ and $T_{\mathbf{g}}$ are related by

$$T_{\mathbf{g}} \;=\; \int_0^S \Omega_{\mathbf{g},1}\,\mathrm{d}s \;=\; \int_0^S \Omega_{\mathbf{f},1} + \dot\theta\,\mathrm{d}s \;=\; T_{\mathbf{f}} + \Delta\theta\,,$$

where $\Delta\theta = \theta(1) - \theta(0)$.

4.2   Adapted frame angle discrepancy on closed curves

Let $(\mathbf{f}_1(\xi), \mathbf{f}_2(\xi), \mathbf{f}_3(\xi))$ be an adapted frame defined on a C^1 closed loop $\mathbf{r}(\xi)$, $\xi \in [\,0, 1\,]$ satisfying

$$\mathbf{r}'(0) \;=\; \mathbf{r}'(1) \quad\text{and}\quad \mathbf{f}_1(0) \;=\; \frac{\mathbf{r}'(0)}{|\mathbf{r}'(0)|} \;=\; \frac{\mathbf{r}'(1)}{|\mathbf{r}'(1)|} \;=\; \mathbf{f}_1(1)\,.$$

In many applications, it is desirable that the entire frame should be periodic along $\mathbf{r}(\xi)$, i.e., we also require that

$$\mathbf{f}_2(0) \;=\; \mathbf{f}_2(1) \quad\text{and}\quad \mathbf{f}_3(0) \;=\; \mathbf{f}_3(1)\,.$$

However, none of the familiar adapted frames — the Frenet frame, ERF, and RMF — are (in general) periodic. To identify a condition for periodicity, we introduce the angle discrepancy of an adapted frame along a closed loop.

Definition 2. *Let $(\mathbf{f}_1, \mathbf{f}_2, \mathbf{f}_3)$ be an adapted frame along a C^1 closed loop $\mathbf{r}(\xi)$, $\xi \in [\,0, 1\,]$. Then the* angle discrepancy D *of $(\mathbf{f}_1, \mathbf{f}_2, \mathbf{f}_3)$ is the unique angle in $[\,0, 2\pi)$ such that*

$$\begin{bmatrix} \mathbf{f}_2(1) \\ \mathbf{f}_3(1) \end{bmatrix} = \begin{bmatrix} \cos D & \sin D \\ -\sin D & \cos D \end{bmatrix} \begin{bmatrix} \mathbf{f}_2(0) \\ \mathbf{f}_3(0) \end{bmatrix},$$

and the frame $(\mathbf{f}_1, \mathbf{f}_2, \mathbf{f}_3)$ is said to be periodic *if its angle discrepancy is zero.*

19

Remark 4. The angle discrepancy of $(\mathbf{f}_1, \mathbf{f}_2, \mathbf{f}_3)$ is the angle from $\mathbf{f}_i(0)$ to $\mathbf{f}_i(1)$ for $i = 2$ or 3, as measured on the coincident normal planes at $\mathbf{r}(0) = \mathbf{r}(1)$ oriented by the common tangent vector $\mathbf{t} = \mathbf{f}_1(0) = \mathbf{f}_1(1)$. This angle can be expressed in terms of the complex argument function as

$$D \;=\; \arg\left[\,\mathbf{f}_i(0) \cdot \mathbf{f}_i(1) + \mathrm{i}\,(\mathbf{f}_i(0) \times \mathbf{f}_i(1)) \cdot \mathbf{f}_1(0)\,\right]$$

for $i = 2$ or 3. Thus, the angle discrepancy D_{FF} of the Frenet frame $(\mathbf{t}, \mathbf{n}, \mathbf{b})$ is obtained directly as

$$\begin{aligned}
D_{\mathrm{FF}} &= \arg\left[\,\mathbf{n}(0) \cdot \mathbf{n}(1) + \mathrm{i}\,(\mathbf{n}(0) \times \mathbf{n}(1)) \cdot \mathbf{t}(0)\,\right] \\
&= \arg\left[\,\mathbf{b}(0) \cdot \mathbf{b}(1) + \mathrm{i}\,(\mathbf{b}(0) \times \mathbf{b}(1)) \cdot \mathbf{t}(0)\,\right] .
\end{aligned}$$

Similarly, the angle discrepancy of the ERF $(\mathbf{e}_1, \mathbf{e}_2, \mathbf{e}_3)$ can be computed from

$$D_{\mathrm{ERF}} \;=\; \arg[\,\mathbf{e}_i(0) \cdot \mathbf{e}_i(1) + \mathrm{i}\,(\mathbf{e}_i(0) \times \mathbf{e}_i(1)) \cdot \mathbf{e}_1(0)\,], \quad i = 2 \ \text{or} \ 3 .$$

We now analyze the relation between the angle discrepancies of two frames using the phase angle function.

Lemma 3. Let $(\mathbf{f}_1, \mathbf{f}_2, \mathbf{f}_3)$ and $(\mathbf{g}_1, \mathbf{g}_2, \mathbf{g}_3)$ be adapted frames on a C^1 closed loop $\mathbf{r}(\xi)$, $\xi \in [0,1]$. If $\theta(\xi)$ is the phase angle function of $(\mathbf{g}_1, \mathbf{g}_2, \mathbf{g}_3)$ relative to $(\mathbf{f}_1, \mathbf{f}_2, \mathbf{f}_3)$, and $D_{\mathbf{f}}$, $D_{\mathbf{g}}$ are the angle discrepancies of these frames, then

$$D_{\mathbf{g}} \;=\; D_{\mathbf{f}} + \Delta\theta \quad \mathrm{mod} \ 2\pi ,$$

where $\Delta\theta = \theta(1) - \theta(0)$.

Proof : By the definition of the angle discrepancy, we have

$$\left[\begin{array}{c} \mathbf{g}_2(1) \\ \mathbf{g}_3(1) \end{array}\right] = \left[\begin{array}{cc} \cos D_{\mathbf{g}} & \sin D_{\mathbf{g}} \\ -\sin D_{\mathbf{g}} & \cos D_{\mathbf{g}} \end{array}\right] \left[\begin{array}{c} \mathbf{g}_2(0) \\ \mathbf{g}_3(0) \end{array}\right] , \tag{35}$$

$$\left[\begin{array}{c} \mathbf{f}_2(1) \\ \mathbf{f}_3(1) \end{array}\right] = \left[\begin{array}{cc} \cos D_{\mathbf{f}} & \sin D_{\mathbf{f}} \\ -\sin D_{\mathbf{f}} & \cos D_{\mathbf{f}} \end{array}\right] \left[\begin{array}{c} \mathbf{f}_2(0) \\ \mathbf{f}_3(0) \end{array}\right] . \tag{36}$$

Moreover, the initial and final orientations of the frame normal–plane vectors are related through the phase angle function by

$$\left[\begin{array}{c} \mathbf{g}_2(0) \\ \mathbf{g}_3(0) \end{array}\right] = \left[\begin{array}{cc} \cos\theta(0) & \sin\theta(0) \\ -\sin\theta(0) & \cos\theta(0) \end{array}\right] \left[\begin{array}{c} \mathbf{f}_2(0) \\ \mathbf{f}_3(0) \end{array}\right] , \tag{37}$$

$$\begin{bmatrix} \mathbf{g}_2(1) \\ \mathbf{g}_3(1) \end{bmatrix} = \begin{bmatrix} \cos\theta(1) & \sin\theta(1) \\ -\sin\theta(1) & \cos\theta(1) \end{bmatrix} \begin{bmatrix} \mathbf{f}_2(1) \\ \mathbf{f}_3(1) \end{bmatrix}. \tag{38}$$

Substituting (37) and (38) into (35), we obtain

$$\begin{bmatrix} \mathbf{f}_2(1) \\ \mathbf{f}_3(1) \end{bmatrix} = \begin{bmatrix} \cos(D_{\mathbf{g}} + \theta(0) - \theta(1)) & \sin(D_{\mathbf{g}} + \theta(0) - \theta(1)) \\ -\sin(D_{\mathbf{g}} + \theta(0) - \theta(1)) & \cos(D_{\mathbf{g}} + \theta(0) - \theta(1)) \end{bmatrix} \begin{bmatrix} \mathbf{f}_2(0) \\ \mathbf{f}_3(0) \end{bmatrix},$$

and comparing this with (36) yields

$$D_{\mathbf{f}} = D_{\mathbf{g}} + \theta(0) - \theta(1) \mod 2\pi. \qquad \blacksquare$$

When a new adapted frame $(\mathbf{g}_1, \mathbf{g}_2, \mathbf{g}_3)$ is constructed from a given adapted frame $(\mathbf{f}_1, \mathbf{f}_2, \mathbf{f}_3)$ and a phase angle function $\theta(\xi)$, the condition for periodicity of $(\mathbf{g}_1, \mathbf{g}_2, \mathbf{g}_3)$ is stated in the following Theorem, which is a straightforward consequence of Lemma 3.

Theorem 1. *Suppose $\theta(\xi)$ is the phase angle function of $(\mathbf{g}_1, \mathbf{g}_2, \mathbf{g}_3)$ relative to $(\mathbf{f}_1, \mathbf{f}_2, \mathbf{f}_3)$. Then the frame $(\mathbf{g}_1, \mathbf{g}_2, \mathbf{g}_3)$ is periodic if and only if*

$$\Delta\theta = \theta(1) - \theta(0) = -D_{\mathbf{f}} + 2k\pi, \quad k \in \mathbb{Z}.$$

For a C^1 closed loop, the RMF is not (in general) periodic. By Lemma 3 with the phase angle $\phi(\xi)$ of the RMF relative to the Frenet frame specified by (33), the angle discrepancy D_{RMF} of the RMF can be expressed as

$$D_{\mathrm{RMF}} = D_{\mathrm{FF}} - \int_0^1 \tau(\xi)\sigma(\xi)\,\mathrm{d}\xi \mod 2\pi.$$

It is noteworthy that the angle discrepancy of the RMF depends on both the angle discrepancy of the Frenet frame and the total torsion. In fact, the total torsion is the twist of the Frenet frame since the angular velocity vector of the Frenet frame — known as the Darboux vector [20] — is

$$\boldsymbol{\omega} = \tau\,\mathbf{t} + \kappa\,\mathbf{b}.$$

We now investigate the relation between the angle discrepancy and the twist of an adapted frame on a closed space curve.

Lemma 4. *Let $(\mathbf{g}_1, \mathbf{g}_2, \mathbf{g}_3)$ be an adapted frame on a C^1 closed loop $\mathbf{r}(\xi)$, $\xi \in [0, 1]$. If $D_{\mathbf{g}}$ and $T_{\mathbf{g}}$ are the angle discrepancy and the twist of $(\mathbf{g}_1, \mathbf{g}_2, \mathbf{g}_3)$ then*

$$D_{\mathbf{g}} = D_{\mathrm{RMF}} + T_{\mathbf{g}} \mod 2\pi,$$

where D_{RMF} is the angle discrepancy of the RMF.

21

Proof : Let $\Omega_{\mathbf{g}} = \Omega_{\mathbf{g},1}\,\mathbf{g}_1 + \Omega_{\mathbf{g},2}\,\mathbf{g}_2 + \Omega_{\mathbf{g},3}\,\mathbf{g}_3$ and $\Omega = \Omega_1\,\mathbf{t} + \Omega_2\,\mathbf{u} + \Omega_3\,\mathbf{v}$ be the angular velocities of the frame $(\mathbf{g}_1, \mathbf{g}_2, \mathbf{g}_3)$ and the RMF, respectively, and let θ be the phase angle of $(\mathbf{g}_1, \mathbf{g}_2, \mathbf{g}_3)$ relative to $(\mathbf{t}, \mathbf{u}, \mathbf{v})$. Then by Lemma 2 we have

$$\Omega_{\mathbf{g},1} = \Omega_1 + \dot{\theta} = \dot{\theta},$$

since the RMF satisfies $\Omega_1 = 0$. Applying Lemma 3 then yields

$$D_{\mathbf{g}} = D_{\mathrm{RMF}} + \Delta\theta = D_{\mathrm{RMF}} + \int_0^S \dot{\theta}\,\mathrm{d}s$$

$$= D_{\mathrm{RMF}} + \int_0^S \Omega_{\mathbf{g},1}\,\mathrm{d}s = D_{\mathrm{RMF}} + T_{\mathbf{g}} \quad \mathrm{mod}\ 2\pi\,. \qquad \blacksquare$$

4.3 C^1 periodic frame on closed loops

In many applications, a C^1 periodic adapted frame $(\mathbf{g}_1, \mathbf{g}_2, \mathbf{g}_3)$ on a C^1 closed curve $\mathbf{r}(\xi)$ is required. When the frame $(\mathbf{g}_1, \mathbf{g}_2, \mathbf{g}_3)$ is constructed by rotation of a given adapted frame $(\mathbf{f}_1, \mathbf{f}_2, \mathbf{f}_3)$ using the phase angle function $\theta(\xi)$, the C^1 periodicity condition can be stated in terms of the initial and the final derivatives of the phase angle function as follows.

Theorem 2. *Suppose* $\theta(\xi)$ *is the phase angle function of* $(\mathbf{g}_1, \mathbf{g}_2, \mathbf{g}_3)$ *relative to* $(\mathbf{f}_1, \mathbf{f}_2, \mathbf{f}_3)$. *Then* $(\mathbf{g}_1, \mathbf{g}_2, \mathbf{g}_3)$ *is a* C^1 *periodic frame if and only if*

$$(a) \quad \Delta\theta = \theta(1) - \theta(0) = -D_{\mathbf{f}} + 2k\pi, \quad k \in \mathbb{Z}$$

$$(b) \quad \dot{\theta}(1) - \dot{\theta}(0) = \Omega_{\mathbf{f},1}(0) - \Omega_{\mathbf{f},1}(1).$$

Proof : In addition to the C^0 periodicity condition (a), the condition (b) is a straightforward consequence of Lemma 2. $\blacksquare$

4.4 Periodic MTF on C^1 PH quintic closed loops

For a C^1 closed–loop PH quintic $\mathbf{r}(\xi)$, $\xi \in [0, 1]$ with the ERF $(\mathbf{e}_1, \mathbf{e}_2, \mathbf{e}_3)$ we wish to construct a periodic MTF $(\mathbf{g}_1, \mathbf{g}_2, \mathbf{g}_3)$ such that

$$\mathbf{g}_2(0) = \mathbf{g}_2(1) = \hat{\mathbf{g}}_2 \quad \text{and} \quad \mathbf{g}_3(0) = \mathbf{g}_3(1) = \hat{\mathbf{g}}_3\,.$$

The initial phase angle $\theta_i = \theta(0)$ is the angle from $\mathbf{e}_2(0)$ to $\hat{\mathbf{g}}_2$, which is chosen in the range $[0, 2\pi)$. From the periodicity condition in Theorem 1, the final phase angle is

$$\theta_f = \theta_i - D_{\mathrm{ERF}} + 2k\pi$$

for some $k \in \mathbb{Z}$. Then the twist $T_{\mathbf{g}}$ of the frame $(\mathbf{g}_1, \mathbf{g}_2, \mathbf{g}_3)$ is

$$T_{\mathbf{g}} = T_{\mathrm{ERF}} + \Delta\theta = T_{\mathrm{ERF}} - D_{\mathrm{ERF}} + 2k\pi \,.$$

To obtain the MTF, we need to choose the integer k for which $T_{\mathbf{g}}$ becomes the reduced minimal twist $T_{\min} \in (-\pi, \pi]$. The mean angular velocity of the MTF is then given by

$$\overline{\Omega}_1 = \frac{T_{\min}}{S} \,.$$

If we do not require the MTF to be rational, we can simply construct it with the constant angular velocity $\overline{\Omega}_1$ by choosing [15] the phase angle function

$$\theta(\xi) = \theta_i + \overline{\Omega}_1 \, s(\xi) - 2 \int_0^\xi \frac{h(t)}{\sigma(t)} \, \mathrm{d}t \,, \tag{39}$$

where $s(\xi)$ is defined by (19)–(20), and the integral admits the closed–form expression (30). This is illustrated by the following examples.

Example 5. For the canonical–form loop in Example 3, the ERF has the initial and final instances

$$(\mathbf{e}_1(0), \mathbf{e}_2(0), \mathbf{e}_3(0)) = (\mathbf{i}, \mathbf{j}, \mathbf{k}) \quad \text{and} \quad (\mathbf{e}_1(1), \mathbf{e}_2(1), \mathbf{e}_3(1)) = (\mathbf{i}, -\mathbf{j}, -\mathbf{k}) \,.$$

Thus, the angle discrepancy of ERF is $D_{\mathrm{ERF}} = \pi$. To construct the periodic MTF $(\mathbf{g}_1, \mathbf{g}_2, \mathbf{g}_3)$ starting with the initial orientation of the ERF, we choose an initial phase angle $\theta_i = 0$ and final phase angle $\theta_f = -D_{\mathrm{ERF}} = -\pi$. The total twist of the periodic frame is

$$T_{\mathbf{g}} = -2.613462 - \pi + 2k\pi \,,$$

and with $k = 1$ we obtain the reduced minimal twist

$$T_{\min} = 0.528131 \,.$$

Since the loop has arc length $S = 1$, the mean angular velocity $\overline{\Omega}_1$ is simply $T_{\min}$. Using the phase angle function computed from (39), we can construct a periodic MTF with constant angular velocity. Figure 8 shows the constructed periodic MTF and the variations of the MTF and ERF angular velocities.
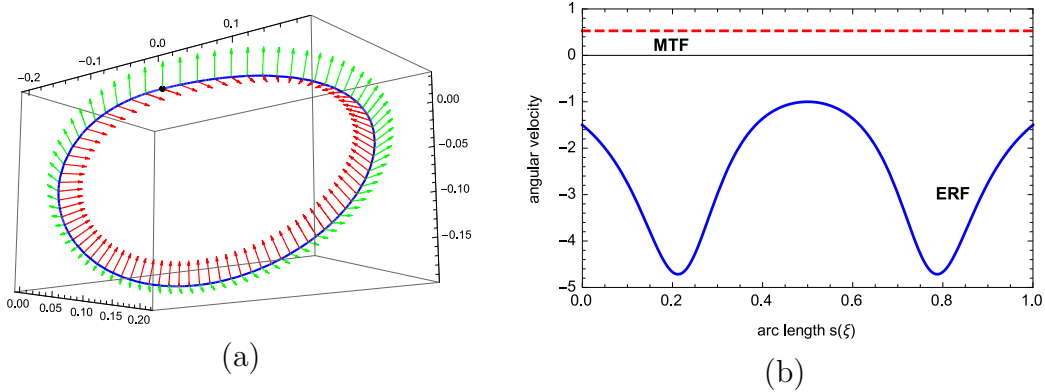
Figure 8: (a) Variation of the vectors $\mathbf{g}_2(\xi)$, $\mathbf{g}_3(\xi)$ of the periodic MTF along the canonical–form loop in Example 3. (b) Graphs of the tangent component of angular velocity for the ERF (solid line) and the MTF (dashed line).

Example 6. Consider the periodic MTF with a constant angular velocity along the canonical–form loop in Example 4. The initial and the final ERF orientations are

$$(\mathbf{e}_1(0), \mathbf{e}_2(0), \mathbf{e}_3(0)) = (\mathbf{i}, -\mathbf{j}, -\mathbf{k}) \quad \text{and} \quad (\mathbf{e}_1(1), \mathbf{e}_2(1), \mathbf{e}_3(1)) = (\mathbf{i}, -\mathbf{k}, \mathbf{j}),$$

and the angle discrepancy is $D_{\text{ERF}} = \pi/2$. To construct the periodic frame, we set $\theta_i = 0$ and $\theta_f = -\pi/2$. The reduced minimal twist (with $k = 0$) is

$$T_{\min} = 1.464840 - \frac{\pi}{2} + 2k\pi = -0.105957,$$

and the mean angular velocity is $\overline{\Omega}_1 = -0.105957$. Using the phase angle function (39), we construct the periodic MTF shown in Figure 9.

5 Rational periodic frames on closed loops

We now consider the possibility of constructing *rational* periodic adapted frames on C^1 PH quintic closed loops, as discussed in Section 3. We adopt the notations in [15] concerning the construction of rational adapted frames on PH curves through rational rotations to the ERF. For a complex polynomial $\mathbf{w}(\xi) = a(\xi) + \mathrm{i}\,b(\xi)$, we associate the phase angle function

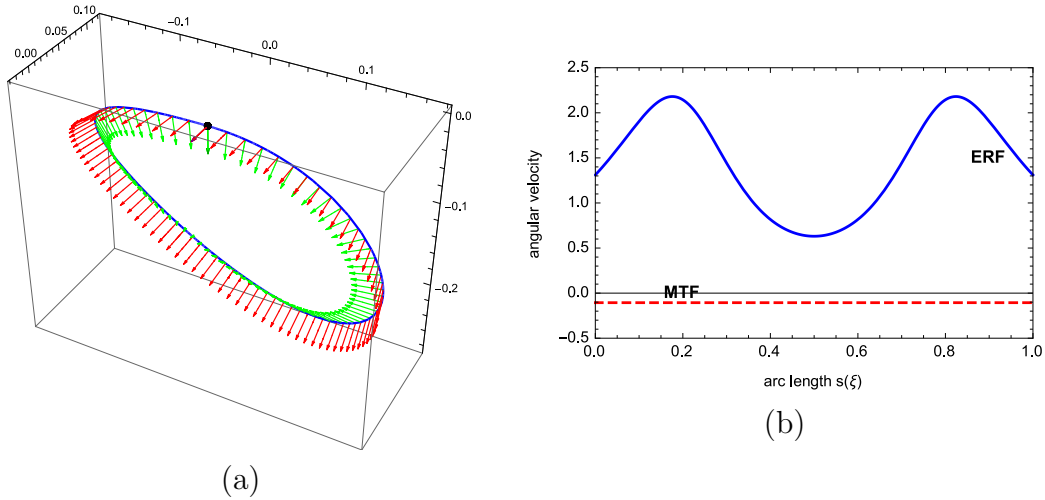$$\theta(\xi) = 2\tan^{-1}\frac{b(\xi)}{a(\xi)}, \tag{40}$$

24

Figure 9: (a) Variation of the vectors $\mathbf{g}_2(\xi)$, $\mathbf{g}_3(\xi)$ of the periodic MTF along the canonical–form loop in Example 4. (b) Graphs of the tangent component of the angular velocity of the ERF (solid line) and the MTF (dashed line).

such that

$$\cos\theta(\xi) \;=\; \frac{a^2(\xi) - b^2(\xi)}{a^2(\xi) + b^2(\xi)}, \quad \sin\theta(\xi) \;=\; \frac{2a(\xi)b(\xi)}{a^2(\xi) + b^2(\xi)},$$

and the rotation (32) specified by the phase angle (40) then has the rational parameterization

$$\left[\begin{array}{c} \mathbf{g}_2(\xi) \\ \mathbf{g}_3(\xi) \end{array} \right] \;=\; \frac{1}{a^2(\xi) + b^2(\xi)} \left[\begin{array}{cc} a^2(\xi) - b^2(\xi) & 2a(\xi)b(\xi) \\ -\,2a(\xi)b(\xi) & a^2(\xi) - b^2(\xi) \end{array} \right] \left[\begin{array}{c} \mathbf{f}_2(\xi) \\ \mathbf{f}_3(\xi) \end{array} \right]. \quad (41)$$

The phase angle can be compactly expressed as

$$\exp(\mathrm{i}\,\theta(\xi)) \;=\; \frac{\mathbf{w}^2(\xi)}{\left|\mathbf{w}(\xi)\right|^2} \;=\; \frac{\mathbf{w}(\xi)}{\overline{\mathbf{w}}(\xi)},$$

and from (40) the derivative of the phase angle function is

$$\theta'(\xi) \;=\; 2\,\frac{a(\xi)b'(\xi) - a'(\xi)b(\xi)}{a^2(\xi) + b^2(\xi)}.$$

In the construction of rational MTFs [15] and of C^1 spline frames [21], quadratic polynomials $\mathbf{w}(\xi)$ were employed. However, a linear polynomial

25

$\mathbf{w}(\xi)$ suffices for constructing C^1 periodic frames along the canonical–form PH quintic closed loops $\mathbf{r}(\xi)$ identified in Section 3. This is possible because of the nice symmetry properties of canonical–form PH quintic closed loops. Let θ_i and θ_f be the initial and the final phase angles of a new frame relative to the ERF. The coefficients of the linear polynomial

$$\mathbf{w}(\xi) = \mathbf{w}_0(1 - \xi) + \mathbf{w}_1\xi$$

are then $\mathbf{w}_0 = \exp(\mathrm{i}\,\frac{1}{2}\theta_i)$, $\mathbf{w}_1 = \gamma\exp(\mathrm{i}\,\frac{1}{2}\theta_f)$ for a real parameter $\gamma \neq 0$ [15].

Proposition 2. *For the canonical–form PH quintic closed loop $\mathbf{r}(\xi)$ with the Bézier control points (17), the adapted frame $(\mathbf{g}_1, \mathbf{g}_2, \mathbf{g}_3)$ obtained by rotating the ERF through the phase angle induced by the linear polynomial*

$$\mathbf{w}(\xi) = \exp\left(\mathrm{i}\tfrac{1}{2}\theta_i\right)(1 - \xi) + \gamma\,\exp\left(\mathrm{i}\tfrac{1}{2}\theta_f\right)\xi \tag{42}$$

becomes a C^1 periodic frame if

$$\theta_f = \theta_i - D_{ERF} + 2k\pi \tag{43}$$

for some $k \in \mathbb{Z}$ and $\gamma = \pm 1$.

Proof : Equation (43) is simply the C^0 periodicity condition. For the C^1 periodicity, we need

$$\Omega_1(0) = \Omega_1(1),$$

where the angular velocity of $(\mathbf{g}_1, \mathbf{g}_2, \mathbf{g}_3)$ is $\mathbf{\Omega}(\xi) = \Omega_1(\xi)\mathbf{g}_1(\xi) + \Omega_2(\xi)\mathbf{g}_2(\xi) + \Omega_3(\xi)\mathbf{g}_3(\xi)$. If $\boldsymbol{\omega}(\xi) = \omega_1(\xi)\mathbf{e}_1(\xi) + \omega_2(\xi)\mathbf{e}_2(\xi) + \omega_3(\xi)\mathbf{e}_3(\xi)$ is the ERF angular velocity, the rotation rates of the normal planes are related by

$$\Omega_1(\xi) = \omega_1(\xi) + \frac{\theta'(\xi)}{\sigma(\xi)}.$$

The parametric speed $\sigma(\xi)$ of the canonical PH quintic loop is symmetric on $[0, 1]$ because of the symmetry of its Bernstein coefficients (18). The angular velocity $\omega_1(\xi) = 2\,h(\xi)/\sigma^2(\xi)$ is also symmetric because $h(\xi)$ defined by (7) is also symmetric. Using $\sigma(0) = \sigma(1)$ and $\omega_1(0) = \omega_1(1)$, the C^1 periodicity condition reduces to $\theta'(0) = \theta'(1)$. For the linear polynomial $\mathbf{w}(\xi)$ in (42), the derivative of the phase angle $\theta(\xi)$ is

$$\theta'(\xi) = \frac{2\,\gamma\sin\frac{1}{2}\Delta\theta}{(1 - \xi)^2 + \gamma\cos\frac{1}{2}\Delta\theta\,2(1 - \xi)\xi + \gamma^2\xi^2}.$$

26

Thus the frame $(\mathbf{g}_1, \mathbf{g}_2, \mathbf{g}_3)$ is C^1 periodic if

$$2\,\gamma \sin \tfrac{1}{2}\Delta\theta \;=\; \frac{2}{\gamma}\sin \tfrac{1}{2}\Delta\theta\,,$$

or equivalently if $\gamma = \pm 1$. $\blacksquare$

We now apply the proposed method with the linear polynomial $\mathbf{w}(\xi)$ to the canonical–form PH quintic loops constructed in Section 3.

Example 7. For the canonical–form loop in Example 3, the initial and the final phase angles are chosen as $\theta_i = 0$ and $\theta_f = -\pi$ for C^0 periodicity. The coefficients of the linear polynomial $\mathbf{w}(\xi)$ are then $\mathbf{w}_0 = 1$ and $\mathbf{w}_1 = -\,\gamma\,\mathrm{i}$, and hence $a(\xi) = 1 - \xi$, $b(\xi) = -\,\gamma\,\xi$. The rational adapted frames obtained by applying the rotation (41) to the ERF have C^1 periodicity for $\gamma = \pm 1$.

The frames constructed by this process are illustrated in Figure 10(a) for $\gamma = 1$ and in Figure 10(b) for $\gamma = -1$. The behavior of the angular velocity of the periodic frames as compared with the ERF are shown in Figure 10(c) for $\gamma = 1$, and in Figure 10(d) for $\gamma = -1$. By virtue of Lemma 1, the ERF angular velocity is always negative. For $\gamma = 1$, the angular velocity of the rational periodic frame is smaller than that of the ERF, so the frame suffers a counter–clockwise twist along the curve, and the total twist is

$$T_{\mathbf{g}} \;=\; -5.755055\,.$$

For $\gamma = -1$, on the other hand, the angular velocity of the rational periodic frame is greater than that of the ERF, with total twist

$$T_{\mathbf{g}} \;=\; 0.528131\,,$$

which agrees with the reduced minimal twist computed in Example 5.

Example 8. Consider the canonical–form loop in Example 4. With the same boundary conditions $\theta_i = 0$ and $\theta_f = -\tfrac{1}{2}\pi$ as in Example 6, C^1 rational periodic frames are constructed with $\gamma = \pm 1$. The variation of the normal–plane vectors is shown in Figure 11(a) for $\gamma = 1$, and Figure 11(b) for $\gamma = -1$. The corresponding angular velocities are plotted Figure 11(c) for $\gamma = 1$ and in Figure 11(d) for $\gamma = -1$. For this example, the twist of each frame is

$$T_{\mathbf{g}} \;=\; -0.105957 \;\; (\gamma = 1) \quad \text{and} \quad T_{\mathbf{g}} \;=\; 6.177228 \;\; (\gamma = -1)\,,$$

so the former has the same value as the reduced minimal twist.
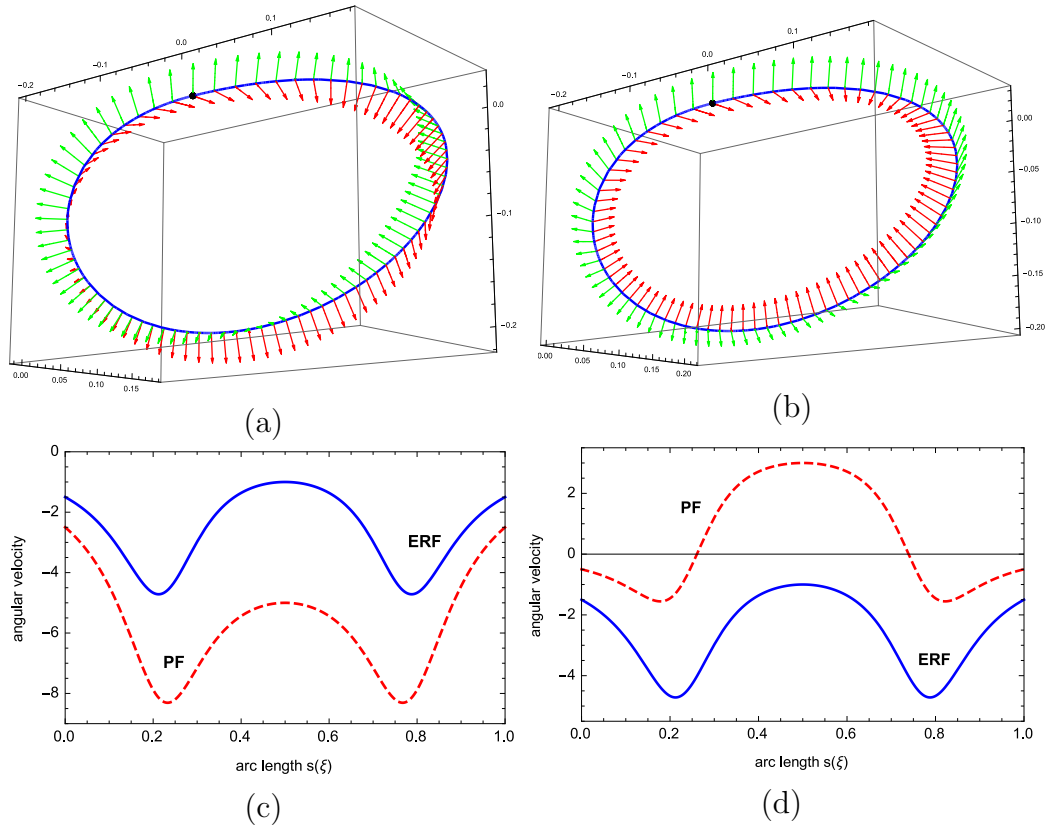
(a)

(b)

(c)

(d)

Figure 10: The rational C^1 periodic frames along the canonical–form loop in Example 3 are illustrated in (a) for $\gamma = 1$, and in (b) for $\gamma = -1$. The angular velocities of the ERF (solid line) and of the periodic frame (dashed line) are compared in (c) for $\gamma = 1$, and in (d) for $\gamma = -1$.
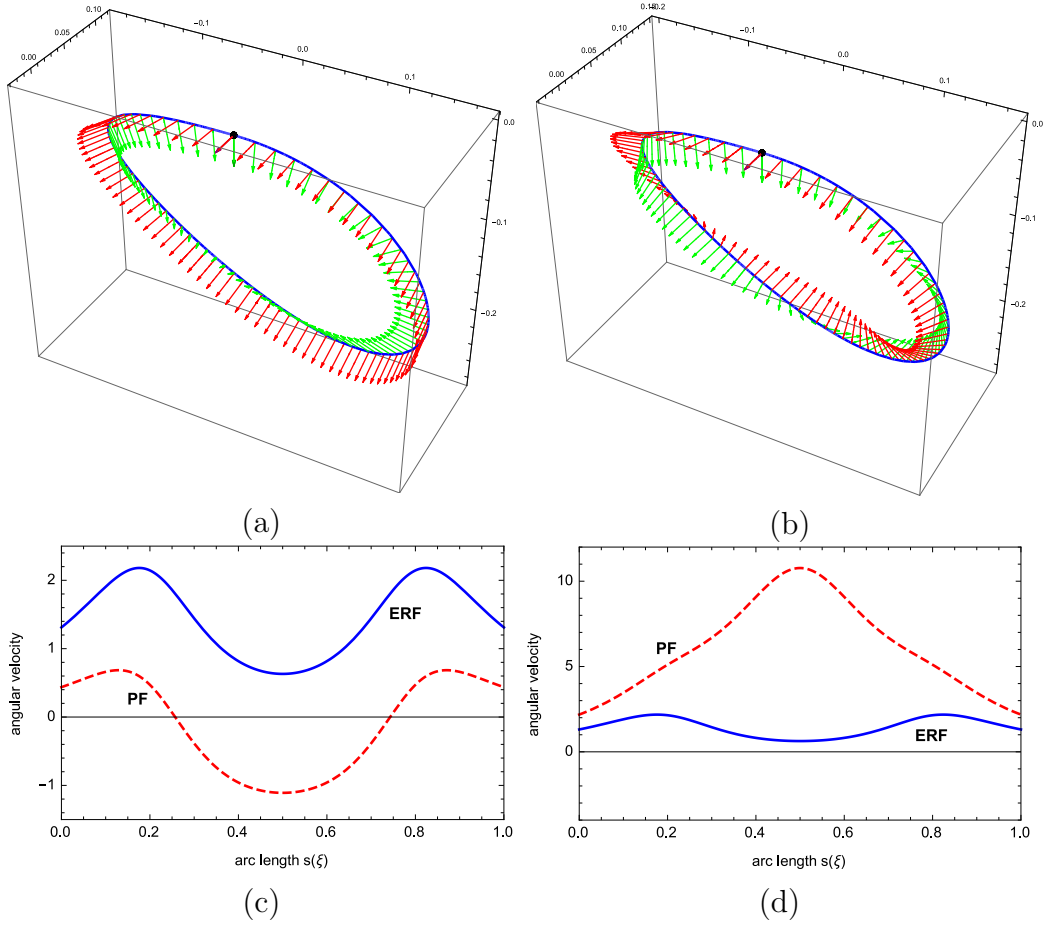
28

(a)

(b)

(c)

(d)

Figure 11: The rational C^1 periodic frames along the canonical–form loop in Example 4 are illustrated in (a) for $\gamma = 1$, and in (b) for $\gamma = -1$. The angular velocities of the ERF (solid line) and of the periodic frame (dashed line) are compared in (c) for $\gamma = 1$, and in (d) for $\gamma = -1$.

6   Closure

The construction of periodic rigid–body motions along closed spatial paths, exhibiting coincident initial and final orientations, is a fundamental problem in spatial kinematics that cannot be solved by familiar orthonormal frames such as the rotation–minimizing frame or Euler–Rodrigues frame on spatial PH curves. The present study develops a framework for the construction of periodic adapted orthonormal frames on C^1 closed–loop paths, and illustrates it in the simplest non–trivial context: the C^1 closed–loop PH quintics.

Several novel concepts and constructs arose in the context of this study. The existence of a two–parameter family of non–planar quintic PH curves that form C^1 closed loops of any prescribed total arc length was established. The theory of continuous adapted orthonormal frames on C^1 closed loops was then developed, based upon a *phase angle* function that describes the relative orientation of two distinct adapted frames, and the *angle discrepancy* for a single adapted frame on a C^1 closed loop. These allow periodic minimal twist frames to be constructed on closed–loop spatial PH curves, using a normal–plane rotation with a transcendental dependence on the curve parameter.

It was further shown that a simple solution for an exact rational periodic adapted frame (though not of minimal twist) on C^1 closed–loop PH quintics is possible. The focus of the present study was to elaborate the basic principles underlying the construction of periodic adapted frames, and to demonstrate their feasibility with simple examples. Two avenues for further investigation come to mind. First, since the C^1 closed–loop PH quintics have limited shape freedoms, algorithms for the construction of higher–order closed–loop PH curves are desirable. Second, the ability to simultaneously achieve rationality, periodicity, and the minimal–twist property of adapted frames on closed loops is the ultimate goal. This is a non–trivial problem, since the ERF, which is typically invoked as a rational adapted "reference" frame, often has a non–monotone angular velocity component in the path tangent direction.

References

[1] M. Barton, B. Jüttler, and W. Wang (2010), Construction of rational curves with rational rotation–minimizing frames via Möbius transformations, in *Mathematical Methods for Curves and Surfaces 2008*, Lecture Notes in Computer Science 5862, 15–25, Springer, Berlin.

[2] R. L. Bishop (1975), There is more than one way to frame a curve, *Amer. Math. Monthly* **82**, 246–251.

[3] H. I. Choi and C. Y. Han (2002), Euler–Rodrigues frames on spatial Pythagorean–hodograph curves, *Comput. Aided Geom. Design* **19**, 603–620.

[4] H. I. Choi, D. S. Lee, and H. P. Moon (2002), Clifford algebra, spin representation, and rational parameterization of curves and surfaces, *Adv. Comp. Math.* **17**, 5–48.

[5] R. T. Farouki (2008), *Pythagorean–Hodograph Curves: Algebra and Geometry Inseparable*, Springer, Berlin.

[6] R. T. Farouki (2010), Quaternion and Hopf map characterizations for the existence of rational rotation–minimizing frames on quintic space curves, *Adv. Comp. Math.* **33**, 331–348.

[7] R. T. Farouki (2016), Rational rotation–minimizing frames — Recent advances and open problems, *Appl. Math. Comp.* **272**, 80–91.

[8] R. T. Farouki (2019), Existence of Pythagorean–hodograph quintic interpolants to spatial G^1 Hermite data with prescribed arc lengths, *J. Symb. Comput.* **95**, 202–216.

[9] R. T. Farouki, M. al–Kandari, and T. Sakkalis (2002), Structural invariance of spatial Pythagorean hodographs, *Comput. Aided Geom. Design* **19**, 395–407.

[10] R. T. Farouki, G. Gentili, C. Giannelli, A. Sestini, and C. Stoppato (2017), A comprehensive characterization of the set of polynomial curves with rational rotation–minimizing frames, *Adv. Comp. Math.* **43**, 1–24.

[11] R. T. Farouki, C. Giannelli, C. Manni, and A. Sestini (2012), Design of rational rotation–minimizing rigid body motions by Hermite interpolation, *Math. Comp.* **81**, 879–903.

[12] R. T. Farouki, C. Giannelli, and A. Sestini (2019), Rational minimal–twist motions on curves with rotation–minimizing Euler–Rodrigues frames, *J. Comput. Appl. Math.* **352**, 240–254.

[13] R. T. Farouki, C. Giannelli, and A. Sestini (2009), Helical polynomial curves and double Pythagorean hodographs I. Quaternion and Hopf map representations, *J. Symb. Comput.* **44**, 161–179.

[14] R. T. Farouki, C. Y. Han, P. Dospra, and T. Sakkalis (2013), Rotation–minimizing Euler–Rodrigues rigid–body motion interpolants, *Comput. Aided Geom. Design* **30**, 653–671.

[15] R. T. Farouki and H. P. Moon (2018), Rational frames of minimal twist along space curves under specified boundary conditions, *Adv. Comp. Math.* **44**, 1627–1650.

[16] R. T. Farouki and T. Sakkalis (2010), Rational rotation–minimizing frames on polynomial space curves of arbitrary degree, *J. Symb. Comput.* **45**, 844–856.

[17] R. T. Farouki and T. Sakkalis (2012), A complete classification of quintic space curves with rational rotation–minimizing frames, *J. Symb. Comput.* **47**, 214–226

[18] H. Guggenheimer (1989), Computing frames along a trajectory, *Comput. Aided Geom. Design* **6**, 77–78.

[19] F. Klok (1986), Two moving coordinate frames for sweeping along a 3D trajectory, *Comput. Aided Geom. Design* **3**, 217–229.

[20] E. Kreyszig (1959), *Differential Geometry*, University of Toronto Press.

[21] H. P. Moon and R. T. Farouki (2018), C^1 and C^2 interpolation of orientation data along spatial Pythagorean–hodograph curves using rational adapted spline frames, *Comput. Aided Geom. Design* **66**, 1–15.

[22] J. V. Uspensky (1948), *Theory of Equations*, McGraw–Hill, New York.